A FRAMEWORK FOR BATCH PROCESSING TRACKLETS IN THE GM-PHD FILTER

A PREPRINT

Dalton Durant*
Department of Aerospace Engineering & Engineering Mechanics
The University of Texas at Austin
Austin, TX 78712
ddurant@utexas.edu

Andrey A. Popov†
Department of Information and Computer Sciences
The University of Hawai'i at Manoa
Manoa, HI 96822
apopov@hawaii.edu

Kyle J. DeMars‡
Department of Aerospace Engineering
Texas A&M University
College Station, TX 77840
demars@tamu.edu

Renato Zanetti§
Department of Aerospace Engineering & Engineering Mechanics
The University of Texas at Austin
Austin, TX 78712
renato@utexas.edu

Code: https://github.com/daltondurant/Batch_GM-PHD.git

ABSTRACT

The objective of this article is to propose a framework for which tracklet data can be batch processed and used within the update step of the Gaussian Mixture Probability Hypothesis Density (GM-PHD) filter. A tracklet represents a sequence of sensor measurements that are associated with the same target over a limited time interval, where if there is high confidence that a tracklet is associated with a true target, it can serve as valuable *a priori* information, helping to reduce the impact of clutter and improve multi-target filtering (MTF) performance. However, traditionally, the GM-PHD filter is not outfitted to handle tracklets within its update step and can only incorporate sensor measurements individually. Therefore, instead of updating recursively with individual sensor measurements, the proposed approach updates the GM-PHD filter's posterior intensity function using tracklets. This article achieves this by pre-processing tracklets into a batch solution of the state space, where the batch solution is then treated as a noisy measurement of the multi-target state. This article uses two different methods for batch processing: Least Squares (LS) for mildly nonlinear and non-Gaussian systems and Markov Chain Monte Carlo (MCMC) with Kernel Density Estimation (KDE) for more complex systems. In the presented radar crossing and cislunar debris tracking examples, the results show that the proposed framework for batch processing tracklets within the GM-PHD filter improves MTF accuracy, demonstrating that they provide more informative updates that reduce the impact of clutter.

Keywords Batch Processing · Tracklets · GM-PHD Filter · Multi-Target Filtering · Least Squares · Markov Chain Monte Carlo

1 Introduction

*Ph.D. Candidate
†Assistant Professor
‡Associate Professor
§Associate Professor

Tracklets are a sequence of sensor measurements that are associated with the same target over a limited time interval. They are typically used in the track fusion community to perform track-level fusion with track filters. Although this article is not directly concerned with track-level fusion or track filtering, it adopts a central idea from prior studies like Carlson [1999], Drummond [1996, 2002], Drummond and Dana-Bashian [2005], Satz and Kerr [2001]. In those works, tracklets of measurements from a local sensor are batch processed into the state space to form track data, which are then used as measurement inputs for a central filter. They find it to be especially useful at the sensor level, where batched tracklets not only reduce the communication load between the sensor and the central filter, but also serve as valuable *a priori* information, helping to improve filtering performance.

In our previous work [Durant et al., 2023], we applied this idea to an orbit determination problem by batch processing tracklets into a mean with covariance using Least Squares (LS) and into Gaussian mixtures using Markov Chain Monte Carlo (MCMC) and Kernel Density Estimation (KDE). We found that batch processing using LS worked well for mildly nonlinear and nearly Gaussian-shaped systems, and MCMC worked better for more complex systems, but was more expensive computationally. Later, in Durant et al. [2024], we extended this to a multi-target tracking problem by performing a data association step after batch processing, followed by a filtering step; however, this proved to be convoluted and slow because of the data association. A more efficient alternative would be to instead use a Random Finite Set (RFS) filter because they do not require an explicit data association step.

Therefore, this article proposes an RFS framework for batch processing tracklets within the Gaussian Mixture Probability Hypothesis Density (GM-PHD) filter [Vo and Ma, 2006]. The GM-PHD filter is of particular interest because it is a popular multi-target filtering (MTF) method, with applications in radar tracking [Qin et al., 2015, Tobias and Lanterman, 2005], computer vision [Eiselein et al., 2012, Pham et al., 2007], autonomous navigation [Lundquist et al., 2010, Leung et al., 2017], and orbit determination [Durant et al., 2025, DeMars and McCabe, 2015, Jones et al., 2015]. However, in its traditional formulation, the GM-PHD filter is not equipped to handle tracklets within its update step and can only incorporate sensor measurements individually. To address this, the proposed approach updates the GM-PHD filter's posterior intensity function by pre-processing tracklets into a batch solution of the state space, where the batch solution is then treated as a noisy measurement of the multi-target state. To apply this to the presented example problems, this article uses the two different methods for batch processing from Durant et al. [2023] and Durant et al. [2024]: LS for mildly nonlinear and nearly Gaussian-shaped systems and MCMC with KDE for more complex systems.

This article is organized as follows. Section 2 gives background to the notation, tracklets, RFS theory, the intensity function, and the GM-PHD filter. Section 3 proposes an RFS framework for batch processing tracklets within the GM-PHD filter, where tracklets are pre-processed into a batch solution of the state space and then treated as noisy measurements of the multi-target state. Additionally, LS and MCMC are presented as two different methods for batch processing tracklets, resulting in the LS GM-PHD filter and the MCMC GM-PHD filter, respectively. Section 4 tests the proposed LS and MCMC GM-PHD filters in a crossing 3D example using radar measurements and in a cislunar debris tracking example using angles-only measurements. The results show that both the LS and MCMC GM-PHD filters improve MTF accuracy, demonstrating that they provide more informative updates and reduce the impact of clutter, compared to the traditional GM-PHD filter. Finally, Section 5 provides a conclusion and discussion of this article's contributions.

2 Background

The goal of this section is to establish the notation used within this article and give background to important concepts like tracklets in Section 2.1, RFS theory in Section 2.2, and the GM-PHD filter recursion as it is traditionally formulated in Section 2.3.

2.1 Tracklets

Suppose we denote $\boldsymbol{x}_k$ as the true state of a single target at some time step k in the state space $\boldsymbol{\mathcal{X}} \subseteq \mathbb{R}^{n_{\boldsymbol{x}}}$ and $\boldsymbol{z}_k$ as a single measurement taken at k in the measurement space $\boldsymbol{\mathcal{Z}} \subseteq \mathbb{R}^{n_{\boldsymbol{z}}}$. Then, let a single-target tracklet be defined to be a sequence of sensor measurements that are associated with the same target over a limited time interval:

$$\boldsymbol{\tau}_k \;\coloneqq\; \{\, \boldsymbol{z}_\ell \,\}_{\ell \in \boldsymbol{\mathcal{I}}_{\boldsymbol{\tau}_k}}, \tag{1}$$

where $\boldsymbol{z}_\ell$ is the measurement at time ℓ and $\boldsymbol{\mathcal{I}}_{\boldsymbol{\tau}_k} \subset \mathbb{N}$ is a finite time index set whose time indices may be irregular and non-consecutive (*e.g.*, $\boldsymbol{\mathcal{I}}_{\boldsymbol{\tau}_k} = \{k, k+1, \ldots, k+T\}$, $\boldsymbol{\mathcal{I}}_{\boldsymbol{\tau}_k} = \{k, k-1, \ldots, k-T\}$ or even $\boldsymbol{\mathcal{I}}_{\boldsymbol{\tau}_k} = \{k+2, k+4 \ldots, k+8\}$). In the multi-target scenario, some sensors are able to convert measurements into multiple tracklets. One example is a time-lapse detection picture produced by an optical telescope, where the pixel data from the image is converted into a tracklet picture, illustrated by Fig. 1. (See Lavezzi [2018] for more information.) In this example, the tracklets may represent sequences of measurements belonging to actual targets or just clutter. Typically, a tracklet is constructed so

that its errors are not cross-correlated with the errors of any other data in the system for the same target. Moreover, a tracklet processing algorithm, like LS or MCMC, does not use any prior information, which results in track data whose errors are also not cross-correlated with those of a central filter.

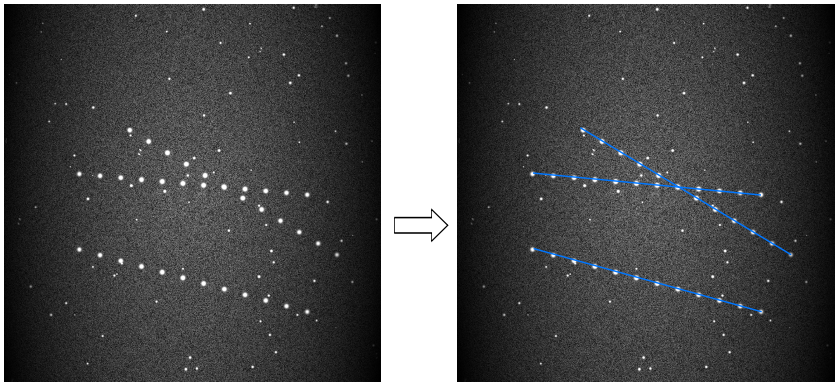

Figure 1: A tracklet picture. Tracking at a sidereal rate, the image is converted into three uncorrelated tracklets. (Parts of this figure were previously presented in an article submitted to the AAS/AIAA Astrodynamics Specialist Conference [Durant et al., 2024], but have not been formally published.)

2.2 Random Finite Set Theory

In the multi-target scenario, suppose N_{k-1} number of targets exist at time step $k-1$, and suppose the target states are $\{\boldsymbol{x}_{k-1,1}, \ldots, \boldsymbol{x}_{k-1,N_{k-1}}\}$. Then, at time k, some of these targets may survive, spawn off of one another, or die, and also some new targets may appear, *i.e.*, birth. This results in an entirely new set of target states $\{\boldsymbol{x}_{k,1}, \ldots, \boldsymbol{x}_{k,N_k}\}$, where N_k is the number of targets at time step k. Since there is no ordering of the target states, they are represented by a finite set:

$$\boldsymbol{X}_k = \{\boldsymbol{x}_{k,1}, \ldots, \boldsymbol{x}_{k,N_k}\} \in \mathcal{F}(\boldsymbol{\mathcal{X}}), \tag{2}$$

where $\mathcal{F}(\boldsymbol{\mathcal{X}})$ is the collection of all finite subsets of $\boldsymbol{\mathcal{X}}$. Additionally, at time k, the sensor provides to the filter a set of M_k measurements $\{\boldsymbol{z}_{k,1}, \ldots, \boldsymbol{z}_{k,M_k}\}$. Similar to the states, the ordering of the measurements do not matter and they are represented by a finite set:

$$\boldsymbol{Z}_k = \{\boldsymbol{z}_{k,1}, \ldots, \boldsymbol{z}_{k,M_k}\} \in \mathcal{F}(\boldsymbol{\mathcal{Z}}), \tag{3}$$

where $\mathcal{F}(\boldsymbol{\mathcal{Z}})$ is the collection of all finite subsets of $\boldsymbol{\mathcal{Z}}$.

The multi-target tracking problem is then formulated as a filtering problem with the multi-target state $\boldsymbol{X}_k$ and multi-target measurement $\boldsymbol{Z}_k$ both modeled as RFSs:

$$\boldsymbol{X}_k = \left[\bigcup_{\boldsymbol{\zeta}\in\boldsymbol{X}_{k-1}} S_{k|k-1}(\boldsymbol{\zeta})\right] \cup \left[\bigcup_{\boldsymbol{\zeta}\in\boldsymbol{X}_{k-1}} B_{k|k-1}(\boldsymbol{\zeta})\right] \cup \Gamma_k, \tag{4}$$

where $S_{k|k-1}(\cdot)$, $B_{k|k-1}(\cdot)$, and Γ_k represent the survival, spawn, and birth RFSs, respectively, and

$$\boldsymbol{Z}_k = K_k \cup \left[\bigcup_{\boldsymbol{x}\in\boldsymbol{X}_k} \Theta_k(\boldsymbol{x})\right], \tag{5}$$

where K_k is the RFS of false measurements, *i.e.*, clutter, and $\Theta_k(\boldsymbol{x})$ is the RFS of target generated measurements, which is either $\{\boldsymbol{z}_k\}$ when a target is detected or $\varnothing$ when not detected.

2.3 The Gaussian Mixture Probability Hypothesis Density Filter

In short, the GM-PHD filter is derived from the Probability Hypothesis Density (PHD) filter [Mahler, 2003], which is based on RFS theory, and is therefore able to handle target survivals, spawns, deaths, and births, while estimating the time-varying number of targets—all in real time. The GM-PHD filter accomplishes these features by only propagating the first-order moment of the full multi-target density, *a.k.a.* the intensity function. The intensity function, denoted by $v(\boldsymbol{x})$, serves as a compact representation of the multi-target density and describes the expected number of targets

at state $\boldsymbol{x}$, scattered randomly in space, according to a Poisson distribution. Its integral over any surveillance region $\mathrm{S} \subseteq \boldsymbol{\mathcal{X}}$ gives the expected number of targets N in that region:

$$N = \int_{\mathrm{S}} v(\boldsymbol{x})\,\mathrm{d}\boldsymbol{x}, \tag{6}$$

where $\mathrm{d}\boldsymbol{x}$ is an infinitesimally small region of $\boldsymbol{x}$ in S. Meaning, the total mass N, *i.e.*, the cardinality, gives the expected number of elements of the RFS $\boldsymbol{X}$.

The GM-PHD filter assumes:

(i) targets evolve independently and generate independent measurements,

(ii) false alarms from clutter are Poisson distributed and are independent of measurements from actual targets,

(iii) the predicted and updated multi-target RFSs are Poisson distributed,

(iv) the dynamics and measurement models are linear Gaussian,

(v) the survival and detection probabilities, $P_{S,k}$ and $P_{D,k}$, are independent of the target state, and

(vi) the birth and spawning intensities are Gaussian mixtures.

Let the linear Gaussian dynamics and measurements be modeled:

$$\boldsymbol{x}_k = \boldsymbol{F}_{k|k-1}\boldsymbol{x}_{k-1} + \boldsymbol{\upsilon}_k, \tag{7}$$

$$\boldsymbol{z}_k = \boldsymbol{H}_k\boldsymbol{x}_k + \boldsymbol{\eta}_k, \tag{8}$$

where $\boldsymbol{F}_{k|k-1}\colon \boldsymbol{\mathcal{X}} \to \boldsymbol{\mathcal{X}}$ denotes the state transition matrix (STM) that maps the state from time step $k-1$ to time step k, and $\boldsymbol{\upsilon}_k \in \boldsymbol{\mathcal{X}}$ is zero-mean white Gaussian process noise with covariance $\boldsymbol{Q}$. Similarly, $\boldsymbol{H}_k\colon \boldsymbol{\mathcal{X}} \to \boldsymbol{\mathcal{Z}}$ denotes the mapping matrix from state space to measurement space, and $\boldsymbol{\eta}_k \in \boldsymbol{\mathcal{Z}}$ is zero-mean white Gaussian measurement noise with covariance $\boldsymbol{R}$, uncorrelated to all $\boldsymbol{\upsilon}_k$.

Given the assumptions (i)–(vi), the GM-PHD approximates the prior intensity as a Gaussian mixture:

$$\begin{aligned} v(\boldsymbol{x}_k) \approx & \underbrace{\sum_{i=1}^{J_{k-1}} P_{S,k} w_{k-1}^{(i)} \mathcal{N}(\boldsymbol{x}_k; \hat{\boldsymbol{x}}_{S,k|k-1}^{(i)}, \hat{\boldsymbol{P}}_{S,k|k-1}^{(i)})}_{\text{survived components}} + \underbrace{\sum_{i=1}^{J_{k-1}} \sum_{j=1}^{J_{\beta,k}} w_{k-1}^{(i)} w_{\beta,k}^{(j)} \mathcal{N}(\boldsymbol{x}_k; \hat{\boldsymbol{x}}_{\beta,k|k-1}^{(i,j)}, \hat{\boldsymbol{P}}_{\beta,k|k-1}^{(i,j)})}_{\text{spawned components}} \\ & + \underbrace{\sum_{i=1}^{J_{\gamma,k}} w_{\gamma,k}^{(i)} \mathcal{N}(\boldsymbol{x}_k; \hat{\boldsymbol{x}}_{\gamma,k}^{(i)}, \hat{\boldsymbol{P}}_{\gamma,k}^{(i)})}_{\text{birthed components}}, \end{aligned} \tag{9}$$

where the subscripts $(\cdot)_S$, $(\cdot)_\beta$, and $(\cdot)_\gamma$ distinguish the survived, spawned, and birthed components, respectively. The notation $\mathcal{N}(\cdot; \boldsymbol{\mu}, \boldsymbol{\Sigma})$ represents the Gaussian distribution with mean $\boldsymbol{\mu}$ and covariance $\boldsymbol{\Sigma}$. Additionally, the hat notation $\hat{(\cdot)}$ is used to indicate variables estimated by the filter and the subscript notation $(\cdot)_{k|k-1}$ is used to denote a predicted estimate from $k-1$ to k. The full expression of (9) can be simplified by setting the total number of components $J_{k|k-1}=J_{k-1}(1+J_{\beta,k})+J_{\gamma,k}$:

$$v(\boldsymbol{x}_k) = \sum_{i=1}^{J_{k|k-1}} w_{k|k-1}^{(i)} p^{(i)}(\boldsymbol{x}_k), \tag{10}$$

where

$$p^{(i)}(\boldsymbol{x}_k) = \mathcal{N}(\boldsymbol{x}_k; \hat{\boldsymbol{x}}_{k|k-1}^{(i)}, \hat{\boldsymbol{P}}_{k|k-1}^{(i)}). \tag{11}$$

Next, given the Gaussian mixture prior intensity in (10), the multi-target measurement $\boldsymbol{Z}_k$, and the assumptions (i)–(vi), the GM-PHD filter has a closed-form analytical solution to the posterior intensity:

$$v(\boldsymbol{x}_k|\boldsymbol{Z}_k) = (1 - P_{D,k}) v(\boldsymbol{x}_k) + \sum_{\boldsymbol{z} \in \boldsymbol{Z}_k} \sum_{i=1}^{J_{k|k-1}} w_{k|k}^{(i)} p^{(i)}(\boldsymbol{x}_k|\boldsymbol{z}), \tag{12}$$

where

$$p^{(i)}(\boldsymbol{x}_k|\boldsymbol{z}) = \mathcal{N}(\boldsymbol{x}_k; \hat{\boldsymbol{x}}_{k|k}^{(i)}, \hat{\boldsymbol{P}}_{k|k}^{(i)}), \tag{13}$$

with

$$\hat{\boldsymbol{x}}_{k|k}^{(i)} = \hat{\boldsymbol{x}}_{k|k-1}^{(i)} + \boldsymbol{K}_k^{(i)}(\boldsymbol{z} - \boldsymbol{H}_k\hat{\boldsymbol{x}}_{k|k-1}^{(i)}), \quad \hat{\boldsymbol{P}}_{k|k}^{(i)} = \hat{\boldsymbol{P}}_{k|k-1}^{(i)} - \boldsymbol{K}_k^{(i)}\boldsymbol{H}_k\hat{\boldsymbol{P}}_{k|k-1}^{(i)},$$
$$\boldsymbol{K}_k^{(i)} = \hat{\boldsymbol{P}}_{k|k-1}^{(i)}\boldsymbol{H}_k^\top(\boldsymbol{S}_k^{(i)})^{-1}, \quad \text{and} \quad \boldsymbol{S}_k^{(i)} = \boldsymbol{H}_k\hat{\boldsymbol{P}}_{k|k-1}^{(i)}\boldsymbol{H}_k^\top + \boldsymbol{R}.$$

The notation $(\cdot)^\top$ is used to represent the matrix transpose and $(\cdot)^{-1}$ the matrix inverse. Additionally, the subscript notation $(\cdot)_{k|k}$ is used to indicate an updated estimate at time step k. The weights also have a closed-form analytical solution:

$$w_{k|k}^{(i)} = \frac{P_{D,k}w_{k|k-1}^{(i)}g^{(i)}(\boldsymbol{z})}{\kappa_k(\boldsymbol{z}) + P_{D,k}\sum_{j=1}^{J_k} w_{k|k-1}^{(j)}g^{(j)}(\boldsymbol{z})}, \tag{14}$$

where

$$g^{(i)}(\boldsymbol{z}) = \mathcal{N}(\boldsymbol{z}; \boldsymbol{H}_k\hat{\boldsymbol{x}}_{k|k-1}^{(i)}, \boldsymbol{S}_k^{(i)}). \tag{15}$$

The notation $\kappa_k(\boldsymbol{z})$ represents the clutter intensity function. Each mixture component in the GM-PHD filter is allowed to evolve according to Bayes' rule, where each Gaussian is interpreted *not* as a posterior PDF, but as a "local" intensity contribution around a hypothesized target state. This allows the means and covariances to be recursively updated individually following the update equations of the Kalman Filter (KF) [Kalman, 1960].

After the update, the number of components grow combinatorially, which the GM-PHD filter manages through a pruning, merging, and capping scheme. Multi-target state extraction is then performed by first estimating the cardinality $\hat{N}_k$ as the sum of the remaining weights, and then selecting the $\hat{N}_k$ components with the highest weights as the estimated target states. Alternatively, they can be chosen to be the components whose weights exceed a prescribed threshold [Vo and Ma, 2006].

However, in the above formulation, the GM-PHD filter cannot directly incorporate tracklets within its update step and can only process individual sensor measurements. This limitation arises from the way the multi-target measurement is modeled, where it contains only the measurements obtained at a single time step. To address this, we seek to reformulate the multi-target measurement model into a multi-target tracklet representation, allowing the GM-PHD filter to use the information contained in each tracklet.

3 Methodology

As already mentioned, the GM-PHD filter is not outfitted to handle tracklets within its update step. To address this, Section 3.1 presents an RFS formulation for the multi-target tracklet, where this formulation assumes that a tracklet consists either of sequences of pure clutter or sequences of true target detections. Then, Section 3.2 derives the GM-PHD filter's posterior intensity function using tracklets instead of individual measurements. Next, Section 3.3 shows that tracklets can instead equivalently be pre-processed into a batch solution of the state space and then treated as noisy measurements of the multi-target state. To obtain the batch solution, we make use of two methods presented in our previous work [Durant et al., 2023, 2024]; as a result, Section 3.4 batch processes tracklets into a mean with covariance using LS and Section 3.5 batch processes tracklets into Gaussian mixtures using MCMC with KDE, resulting in the LS GM-PHD filter and the MCMC GM-PHD filter, respectively.

3.1 An RFS Formulation for the Multi-Target Tracklet

Instead of individual measurements at time k, consider that the sensor provides to the filter a set of M_k tracklets $\{\boldsymbol{\tau}_{k,1}, \ldots, \boldsymbol{\tau}_{k,M_k}\}$, where $\boldsymbol{\tau} \in \boldsymbol{\mathcal{T}}$, and $\boldsymbol{\mathcal{T}} \subseteq \mathbb{R}^{n_{\boldsymbol{z}}}$ is the tracklet space. Similar to the set of individual measurements, the ordering of the tracklets does not matter and they are represented by a finite set:

$$\boldsymbol{T}_k = \{\boldsymbol{\tau}_{k,1}, \ldots, \boldsymbol{\tau}_{k,M_k}\} \in \mathcal{F}(\boldsymbol{\mathcal{T}}), \tag{16}$$

where $\mathcal{F}(\boldsymbol{\mathcal{T}})$ is the collection of all finite subsets of $\boldsymbol{\mathcal{T}}$. Then, given the multi-target state $\boldsymbol{X}_k$ at time k, the multi-target tracklet $\boldsymbol{T}_k$ is formed by the union of clutter and the target generated tracklets:

$$\boldsymbol{T}_k = K_k \cup \left[\bigcup_{\boldsymbol{x}\in\boldsymbol{X}_k} \Theta_k(\boldsymbol{x})\right], \tag{17}$$

where K_k now represents the RFS of clutter over the entire tracklet interval (*i.e.*, the RFS of clutter at all measurement times within the tracklet), and $\Theta_k(\boldsymbol{x})$ now is the RFS of target generated tracklets, which is either $\{\boldsymbol{\tau}_k\}$ when a target is detected or $\varnothing$ when not detected. This means that tracklets of apparent targets are assumed to either only contain sequences of pure clutter or sequences of true target detections.

3.2 Derivation for the GM-PHD Filter Update Step Using Tracklets

One key aspect of the PHD filter's posterior intensity function in Mahler [2003] is that it hinges on the likelihood. In the GM-PHD filter derivation from Vo and Ma [2006], the authors make the assumption that the predicted Gaussian components and their respective likelihood functions are all Gaussian. This means that if the system has linear Gaussian dynamics and measurements, then the GM-PHD filter has a closed-form analytical solution to the posterior intensity per scan, *i.e.*, per update step, as seen in (12). Therefore, under the same linear Gaussian conditions, the following derives a closed-form analytical solution to the posterior intensity using tracklets instead of individual measurements.

To convey the basic principles of the proposed methods, the following mathematical equations omit process noise. However, they can, in theory, be extended to include process noise without significant difficulty, where the main results of this section still remain valid even when it is included. Therefore, let the likelihood of a tracklet given the target state be:

$$\begin{aligned} g(\boldsymbol{\tau}_k|\boldsymbol{x}_k) &= \prod_{\ell \in \boldsymbol{\mathcal{I}}_{\boldsymbol{\tau}_k}} \mathcal{N}(\boldsymbol{z}_\ell; \boldsymbol{H}_\ell \boldsymbol{F}_{\ell|k} \boldsymbol{x}_k, \boldsymbol{R}) \\ &= \mathcal{N}(\boldsymbol{\tau}_k; \mathbf{H}_k \mathbf{F}_k \boldsymbol{x}_k, \mathbf{R}), \end{aligned} \tag{18}$$

where the straightened variables $\mathbf{F}_k$ and $\mathbf{H}_k$ represent vertical stacks of the matrices $\boldsymbol{F}_{\ell|k}$ and $\boldsymbol{H}_\ell$, respectively, for all $\ell \in \boldsymbol{\mathcal{I}}_{\boldsymbol{\tau}_k}$. In a similar fashion, the straightened $\mathbf{R}$ represents the block diagonal matrix of $\boldsymbol{R}$. In the above likelihood formulation, we are assuming that process noise is zero. However, if (18) we were to include process noise, then the likelihood function would become:

$$g(\boldsymbol{\tau}_k|\boldsymbol{x}_k) = \prod_{\ell \in \boldsymbol{\mathcal{I}}_{\boldsymbol{\tau}_k}} \mathcal{N}(\boldsymbol{z}_\ell; \boldsymbol{H}_\ell \boldsymbol{F}_{\ell|k} \boldsymbol{x}_k, \boldsymbol{H}_\ell \boldsymbol{F}_{\ell|k} \boldsymbol{Q} \boldsymbol{F}_{\ell|k}^\top \boldsymbol{H}_\ell^\top + \boldsymbol{R}).$$

Moreover, we are also assuming all measurements within a tracklet are conditionally independent given the target state. This assumption is consistent with the track fusion literature, where tracklets are constructed so that their errors are not cross-correlated with those of other data for the same target. In practice, however, the pre-processing steps used to form tracklets can introduce statistical dependencies among measurements, which could, in principle, lead to overconfident likelihood estimates if independence were strictly enforced. In this work, the independence assumption in (18) is adopted primarily for notational simplicity, while the later parts of this section (Section 3.4 and Section 3.5) mitigate this issue by compressing each tracklet into a single batch observation, represented either by a mean and covariance or by a Gaussian mixture, which implicitly accounts for the internal correlations.

With that said, we can substitute (18) into Bayes' rule:

$$g(\boldsymbol{\tau}_k|\boldsymbol{x}_k)\, p^{(i)}(\boldsymbol{x}_k) = p^{(i)}(\boldsymbol{x}_k|\boldsymbol{\tau}_k)\, g^{(i)}(\boldsymbol{\tau}_k) \tag{19}$$

and compute the integral of the measurement marginal:

$$\begin{aligned} g^{(i)}(\boldsymbol{\tau}_k) &= \int g(\boldsymbol{\tau}_k|\boldsymbol{x}_k)\, p^{(i)}(\boldsymbol{x}_k)\, \mathrm{d}\boldsymbol{x}_k \\ &= \mathcal{N}(\boldsymbol{\tau}_k; \mathbf{H}_k \mathbf{F}_k \hat{\boldsymbol{x}}_{k|k-1}^{(i)}, \mathbf{S}_k^{(i)}), \end{aligned} \tag{20}$$

where

$$\mathbf{S}_k^{(i)} = \mathbf{H}_k \mathbf{F}_k \hat{\boldsymbol{P}}_{k|k-1}^{(i)} \mathbf{F}_k^\top \mathbf{H}_k^\top + \mathbf{R}.$$

Then, the posterior becomes:

$$p^{(i)}(\boldsymbol{x}_k|\boldsymbol{\tau}_k) = \mathcal{N}(\boldsymbol{x}_k; \hat{\boldsymbol{x}}_{k|k}^{(i)}, \hat{\boldsymbol{P}}_{k|k}^{(i)}), \tag{21}$$

where

$$\hat{\boldsymbol{x}}_{k|k}^{(i)} = \hat{\boldsymbol{x}}_{k|k-1}^{(i)} + \boldsymbol{K}_k^{(i)}(\boldsymbol{\tau}_k - \mathbf{H}_k \mathbf{F}_k \hat{\boldsymbol{x}}_{k|k-1}^{(i)}), \quad \hat{\boldsymbol{P}}_{k|k}^{(i)} = \hat{\boldsymbol{P}}_{k|k-1}^{(i)} - \boldsymbol{K}_k^{(i)} \mathbf{H}_k \mathbf{F}_k \hat{\boldsymbol{P}}_{k|k-1}^{(i)}, \quad \text{and}$$
$$\boldsymbol{K}_k^{(i)} = \hat{\boldsymbol{P}}_{k|k-1}^{(i)} \mathbf{F}_k^\top \mathbf{H}_k^\top (\mathbf{S}_k^{(i)})^{-1}.$$

The posterior solution in (21) is the linear batch Kalman filter update, where its mean is both exactly the Minimum Mean Squared Error (MMSE) and *Maximum a Posteriori* (MAP) estimate. Finally, given the Gaussian mixture prior intensity from (10), the multi-target tracklet $\boldsymbol{T}_k$, and conditions (i)–(vi), the GM-PHD filter has a closed-form analytical solution to the posterior intensity:

$$v(\boldsymbol{x}_k|\boldsymbol{T}_k) = (1 - P_{D,k}) v(\boldsymbol{x}_k) + \sum_{\boldsymbol{\tau} \in \boldsymbol{T}_k} \sum_{i=1}^{J_{k|k-1}} w_{k|k}^{(i)} p^{(i)}(\boldsymbol{x}_k|\boldsymbol{\tau}), \tag{22}$$

where

$$w_{k|k}^{(i)} \;=\; \frac{P_{D,k} w_{k|k-1}^{(i)} g^{(i)}(\boldsymbol{\tau})}{\kappa_k(\boldsymbol{\tau}) \;+\; P_{D,k} \sum_{j=1}^{J_k} w_{k|k-1}^{(j)} g^{(j)}(\boldsymbol{\tau})}. \tag{23}$$

Remark 1. *By using tracklets, the GM-PHD filter provides estimates at a single update time, and it is therefore the responsibility of the operator to obtain the estimates at the times throughout the remainder of the tracklet interval, either through propagation of the mixture components or through other means. The actual process of this is very much problem dependent; some examples are presented in Section 4.*

Remark 2. *The function $\kappa_k(\boldsymbol{\tau})$ does not represent the clutter intensity over a single scan, but rather over an entire tracklet. In other words, it represents the intensity that an entire sequence of measurements $\boldsymbol{\tau}$ was generated by the clutter process rather than by a target. For a single scan, this is straightforward and reduces to $\kappa_k(\boldsymbol{\tau}) = \lambda_C\, p_C(\boldsymbol{z})$ when $\boldsymbol{\tau} = \boldsymbol{z}$. However, for a multi-scan tracklet, computing $\kappa_k(\boldsymbol{\tau})$ would require the probability that all measurements in the sequence are clutter and that they occur in a manner consistent with building a tracklet. Since clutter is modeled as independent and identically distributed (i.i.d.) in time, the GM-PHD filter framework provides no temporal model for clutter; as a result, computing such a probability would require integrating over all possible spatial and temporal configurations of clutter that could form a valid tracklet. This is analytically intractable, and therefore $\kappa_k(\boldsymbol{\tau})$ must be approximated.*

Approximating $\kappa_k(\boldsymbol{\tau})$ can be done by making modeling assumptions. For example, consider a simple modeling assumption that shorter tracklets are more likely to be clutter than longer ones. In this case, a relationship can be formed between the clutter intensity $\kappa_k(\boldsymbol{\tau})$ and the tracklet length $|\boldsymbol{\tau}|$:

$$\kappa_k(\boldsymbol{\tau}) \approx \begin{cases} \mathrm{a}_k, & \text{if } |\boldsymbol{\tau}| < \mathrm{b}_k \\ \mathrm{c}_k\, |\boldsymbol{\tau}|^{-\mathrm{d}_k}, & \text{otherwise} \end{cases}, \tag{24}$$

where a_k, b_k, c_k, and d_k are heuristic parameters. In this piecewise function, when $|\boldsymbol{\tau}|$ is smaller than b_k, the clutter intensity is a large value a_k; otherwise, when $|\boldsymbol{\tau}|$ is larger than or equal to b_k, the clutter intensity decreases rapidly as a power-law function of $|\boldsymbol{\tau}|$ with exponent $\mathrm{d}_k{>}1$ and multiplier c_k. In other words, shorter tracklets are likely to be clutter and longer tracklets are increasingly unlikely to be clutter. This form is used in the examples presented in Section 4.

3.3 Alternative Derivation: Pre-Processing Tracklets into a Batch Solution of the State Space for the GM-PHD Filter

Theorem 1. *If the GM-PHD filter conditions (i)–(vi) hold and the multi-target tracklet $\boldsymbol{T}_k$ is given, and assuming negligible process noise such that the associated likelihood can be expressed as (18), then the GM-PHD filter update equations (22)–(23) admit an alternative, mathematically equivalent formulation. This equivalent form, given by (29)–(30), is obtained by pre-processing the tracklets into a batch estimate in the state space and treating the resulting estimates as noisy measurements of the multi-target state.*

Proof. First, let the likelihood from (18) be reformulated:

$$\begin{aligned} g(\boldsymbol{\tau}_k|\boldsymbol{x}_k) &= \prod_{\ell \in \boldsymbol{\mathcal{I}}_{\boldsymbol{\tau}_k}} \mathcal{N}(\boldsymbol{z}_\ell; \boldsymbol{H}_\ell \boldsymbol{F}_{\ell|k} \boldsymbol{x}_k, \boldsymbol{R}) \\ &= \mathcal{N}(\boldsymbol{\tau}_k; \mathbf{H}_k \mathbf{F}_k \boldsymbol{x}_k, \mathbf{R}) \\ &= C_k\, \mathcal{N}(\boldsymbol{x}_k; \tilde{\boldsymbol{x}}_k, \tilde{\boldsymbol{P}}_k) \\ &= C_k\, g(\tilde{\boldsymbol{x}}_k|\boldsymbol{x}_k), \end{aligned} \tag{25}$$

where

$$\tilde{\boldsymbol{x}}_k = \tilde{\boldsymbol{P}}_k \mathbf{F}_k^\top \mathbf{H}_k^\top \mathbf{R}^{-1}\, \boldsymbol{\tau}_k, \quad \tilde{\boldsymbol{P}}_k = \left(\mathbf{F}_k^\top \mathbf{H}_k^\top \mathbf{R}^{-1} \mathbf{H}_k \mathbf{F}_k\right)^{-1}, \quad \text{and} \quad C_k = \frac{1}{\prod_{\ell \in \boldsymbol{\mathcal{I}}_{\boldsymbol{\tau}_k}} \det(2\pi \boldsymbol{R})^{1/2}}.$$

The notation $\tilde{\boldsymbol{x}}_k$ and $\tilde{\boldsymbol{P}}_k$ represent the entire tracklet in the state space batch processed into a single mean with covariance, respectively, following the Maximum Likelihood Estimate (MLE) equations from B. Schutz [2004]. While trivial, a deeper look into this operation reveals that the measurement information of the entire tracklet has been re-factored from the measurement space into the state space; this requires $\tilde{\boldsymbol{P}}_k$ to be invertible, thereby connecting the length of the tracklet to the observability of the system.

Next, by substituting (25) into Bayes' rule, this gives:

$$\begin{aligned} p^{(i)}(\boldsymbol{x}_k|\boldsymbol{\tau}_k)\; g^{(i)}(\boldsymbol{\tau}_k) &= g(\boldsymbol{\tau}_k|\boldsymbol{x}_k)\; p^{(i)}(\boldsymbol{x}_k) \\ &= C_k\; g(\tilde{\boldsymbol{x}}_k|\boldsymbol{x}_k)\; p^{(i)}(\boldsymbol{x}_k) \\ &= C_k\; p^{(i)}(\boldsymbol{x}_k|\tilde{\boldsymbol{x}}_k)\; g^{(i)}(\tilde{\boldsymbol{x}}_k). \end{aligned} \tag{26}$$

The measurement marginal $g^{(i)}(\tilde{\boldsymbol{x}}_k)$ can be computed analytically:

$$\begin{aligned} g^{(i)}(\tilde{\boldsymbol{x}}_k) &= \int g(\tilde{\boldsymbol{x}}_k|\boldsymbol{x}_k)\; p^{(i)}(\boldsymbol{x}_k)\; \mathrm{d}\boldsymbol{x}_k \\ &= \mathcal{N}(\tilde{\boldsymbol{x}}_k; \hat{\boldsymbol{x}}^{(i)}_{k|k-1}, \hat{\boldsymbol{P}}^{(i)}_{k|k-1} + \tilde{\boldsymbol{P}}_k), \end{aligned} \tag{27}$$

Also, the posterior $p^{(i)}(\boldsymbol{x}_k|\tilde{\boldsymbol{x}}_k)$ can be computed analytically:

$$p^{(i)}(\boldsymbol{x}_k|\tilde{\boldsymbol{x}}_k) = \mathcal{N}(\boldsymbol{x}_k; \hat{\boldsymbol{x}}^{(i)}_{k|k}, \hat{\boldsymbol{P}}^{(i)}_{k|k}), \tag{28}$$

where now

$$\hat{\boldsymbol{x}}^{(i)}_{k|k} = \hat{\boldsymbol{x}}^{(i)}_{k|k-1} + \boldsymbol{K}^{(i)}_k(\tilde{\boldsymbol{x}}_k - \hat{\boldsymbol{x}}^{(i)}_{k|k-1}), \quad \hat{\boldsymbol{P}}^{(i)}_{k|k} = \hat{\boldsymbol{P}}^{(i)}_{k|k-1} - \boldsymbol{K}^{(i)}_k \hat{\boldsymbol{P}}^{(i)}_{k|k-1}, \quad \text{and} \quad \boldsymbol{K}^{(i)}_k = \hat{\boldsymbol{P}}^{(i)}_{k|k-1}(\hat{\boldsymbol{P}}^{(i)}_{k|k-1} + \tilde{\boldsymbol{P}}_k)^{-1}.$$

Finally, substituting (28) and (27) into (22) and (23), respectively, results in a GM-PHD filter with an alternative closed-form analytical solution to the posterior intensity:

$$v(\boldsymbol{x}_k|\boldsymbol{T}_k) = (1 - P_{D,k})v(\boldsymbol{x}_k) + \sum_{\boldsymbol{\tau}\in\boldsymbol{T}_k} \sum_{i=1}^{J_{k|k-1}} w^{(i)}_{k|k} p^{(i)}(\boldsymbol{x}_k|\tilde{\boldsymbol{x}}_k), \tag{29}$$

where

$$w^{(i)}_{k|k} = \frac{P_{D,k} w^{(i)}_{k|k-1} C_k\; g^{(i)}(\tilde{\boldsymbol{x}}_k)}{\kappa_k(\boldsymbol{\tau}) + P_{D,k} \sum_{j=1}^{J_k} w^{(j)}_{k|k-1} C_k\; g^{(j)}(\tilde{\boldsymbol{x}}_k)}. \tag{30}$$

Since (25) holds for linear Gaussian systems, the intensity function and its weights in (22) and (23) are exactly equal to that of (29) and (30), respectively.

This is the end of the proof. □

3.4 Using Least Squares to Batch Process Tracklets in the GM-PHD Filter

For nonlinear systems, there no longer exists closed-form analytical solutions for (25)–(30). Let dynamics and measurement models now be modeled as nonlinear:

$$\boldsymbol{x}_k = f_{k|k-1}(\boldsymbol{x}_{k-1}) + \boldsymbol{\upsilon}_k, \tag{31}$$

$$\boldsymbol{z}_k = h(\boldsymbol{x}_k) + \boldsymbol{\eta}_k, \tag{32}$$

where $f_{k|k-1}(\cdot)\colon \boldsymbol{\mathcal{X}} \to \boldsymbol{\mathcal{X}}$ is the nonlinear discrete dynamics propagation function that propagates the state from time step $k-1$ to time step k, and $h(\cdot)\colon \boldsymbol{\mathcal{X}} \to \boldsymbol{\mathcal{Z}}$ is the nonlinear measurement function. Although closed form analytical solutions no longer exist, LS can be used to solve a nonlinear cost function, finding the best batch solution through optimization. Therefore, LS can be used to batch each tracklet $\boldsymbol{\tau}_k$ into a single mean with covariance in the state space. This optimized batch solution can then be treated as the uncorrelated noisy observation of the multi-target state, by which it can then be used to obtain approximations for (27)–(30). Fig. 2 illustrates this approach.

In step 2 of Fig. 2, given a problem specific proposal mean $\boldsymbol{x}^{\text{Prop.}}_k$ with covariance $\boldsymbol{P}^{\text{Prop.}}_k$, LS solves the following cost function for $\boldsymbol{x}_k$:

$$\min_{\boldsymbol{x}_k}\Big\{\frac{1}{2}(\boldsymbol{x}_k - \boldsymbol{x}^{\text{Prop.}}_k)^\top (\boldsymbol{P}^{\text{Prop.}}_k)^{-1}(\boldsymbol{x}_k - \boldsymbol{x}^{\text{Prop.}}_k) + \sum_{\ell\in\boldsymbol{T}_{\boldsymbol{\tau}_k}} \frac{1}{2}\big(\boldsymbol{z}_\ell - h(f_{\ell|k}(\boldsymbol{x}_k))\big)^\top (\boldsymbol{R})^{-1}\big(\boldsymbol{z}_\ell - h(f_{\ell|k}(\boldsymbol{x}_k))\big)\Big\} \tag{33}$$

The resulting LS batch solution converges to a mean $\tilde{\boldsymbol{x}}_k$ with a covariance $\tilde{\boldsymbol{P}}_k$. Finally, in step 3 of Fig. 2, the posterior intensity is approximated by substituting the mean $\tilde{\boldsymbol{x}}_k$, covariance $\tilde{\boldsymbol{P}}_k$, and an approximation for C_k into (27)–(30).

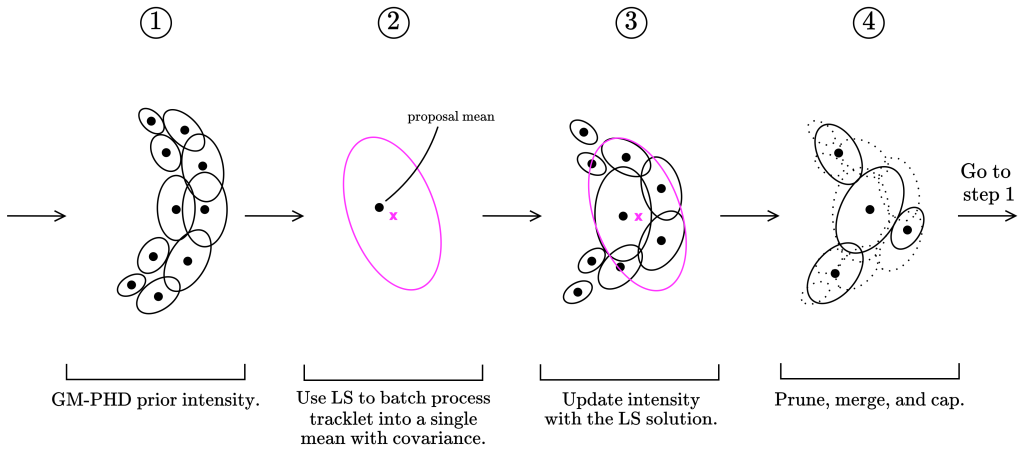

Figure 2: Flowchart of the LS GM-PHD filter. Step 1 constructs the prior intensity in the traditional manner using (10). Then, step 2 computes the batch solution using (33). Next, step 3 uses the batch solution as measurement input for the GM-PHD filter and updates using (27)–(30). Finally, step 4 performs pruning, merging, and capping like it is traditionally done in the GM-PHD filter.

Remark 3. *Generally, $\boldsymbol{P}_k^{Prop.}$ is not a realistic representation of the accuracy of $\boldsymbol{x}_k^{Prop.}$. Ideally, the proposal distribution should be chosen to be diffuse: $\boldsymbol{P}_k^{Prop.} \to \infty$, indicating no prior information about the tracklet is known. This ensures that the batch solution is uncorrelated to the filter estimates when it is used as noisy observations. But, in practice, the proposal covariance is chosen to be a large-valued diagonal matrix to provide a stable batch solution, as remarked by B. Schutz [2004]. Therefore, the first term in (33) will be very small and the measurement residuals will drive the cost function.*

Remark 4. *Just how there exists no analytical solutions for $\tilde{\boldsymbol{x}}_k$ and $\tilde{\boldsymbol{x}}_k$, there neither exists analytical solutions for the normalization constant C_k. However, there are some options for dealing with it:*

1. *approximate C_k using the linear Gaussian assumptions, or*
2. *assume that C_k gets captured into the clutter intensity: $\kappa_k(\boldsymbol{\tau}) \leftarrow C_k \kappa_k(\boldsymbol{\tau})$, which allows it to cancel on the numerator and denominator of (30).*

3.5 Using Markov Chain Monte Carlo to Batch Process Tracklets in the GM-PHD Filter

In our previous work [Durant et al., 2023, 2024], we found that the LS approach performed well for systems whose dynamics and measurement models are mildly nonlinear and probability distributions are well approximated by a single Gaussian. However, when system dynamics and measurement models are more nonlinear, LS is unable to capture the non-Gaussian structure of the uncertainty with a single mean and covariance. To address this, we proposed batch processing tracklets into Gaussian mixtures using MCMC with KDE. MCMC algorithms, such as Metropolis-Hastings (M-H) [Metropolis et al., 1953, Hastings, 1970] and Hamiltonian Monte Carlo (HMC) [Neal, 2011], were used to draw i.i.d. samples from a complex target likelihood distribution like $\frac{1}{C_k} g(\boldsymbol{\tau}_k|\boldsymbol{x}_k)$, without requiring C_k itself. KDE was used to transform the MCMC samples into a Gaussian mixture. While this approach was computationally more expensive than LS, it was able to accurately preserve non-Gaussian uncertainty structures and multimodality. This is because Gaussian mixtures are effective at accurately approximating any distribution arbitrarily well in their limit of components. Therefore, the approach is adapted here for the GM-PHD filter, where Fig. 3 illustrates this process.

In step 2 of Fig. 3, M i.i.d. samples $\{\boldsymbol{\mathcal{D}}_k^{(j)}\}_{j=1}^M$ are drawn from the target likelihood distribution $\frac{1}{C_k} g(\boldsymbol{\tau}_k|\boldsymbol{x}_k)$ given some problem specific proposal distribution. After which, they can be expressed as a uniformly weighted Dirac mixture:

$$C_k \; g(\tilde{\boldsymbol{x}}_k|\boldsymbol{x}_k) \approx \sum_{j=1}^{M} \frac{1}{M} \delta(\boldsymbol{x}_k - \boldsymbol{\mathcal{D}}_k^{(j)}), \tag{34}$$

where $\delta(\cdot)$ denotes the Dirac delta distribution, which can be interpreted as a Gaussian with covariance approaching the zero matrix in the limit. Then, in step 3 of Fig. 3, to convert this Dirac mixture into a tractable Gaussian mixture, the

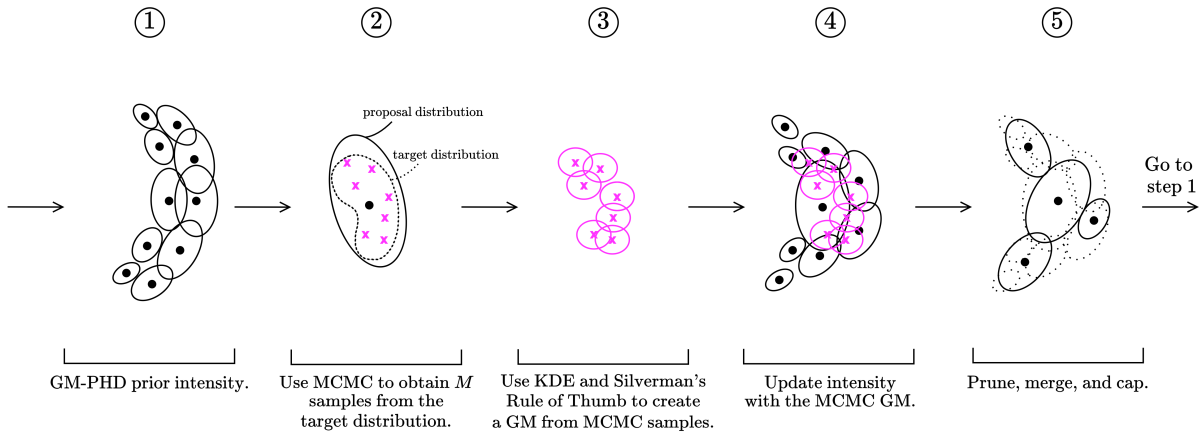

Figure 3: Flowchart of the MCMC GM-PHD filter. Step 1 constructs the prior intensity in the traditional manner using (10). Then, step 2 generates a batch solution in the form of MCMC samples, represented by the Dirac mixture in (34). Step 3 then converts this Dirac mixture into a Gaussian mixture using (35)–(38). Next, step 4 uses the Gaussian mixture batch solution as measurement input for the GM-PHD filter and updates using (39)–(41). Finally, step 5 performs pruning, merging, and capping like it is traditionally done in the GM-PHD filter.

KDE method from Silverman [2018] is applied, where each sample is transformed into a Gaussian component with nonzero covariance and equal weight:

$$C_k\, g(\tilde{\boldsymbol{x}}_k|\boldsymbol{x}_k) \approx \sum_{j=1}^{M} \frac{1}{M} \mathcal{N}\big(\boldsymbol{x}_k; \boldsymbol{\mathcal{D}}_k^{(j)}, \boldsymbol{B}_k\big), \tag{35}$$

and all components share the same bandwidth covariance matrix:

$$\boldsymbol{B}_k = \beta_{\text{Silv.}} \text{Cov}(\{\boldsymbol{\mathcal{D}}_k^{(j)}\}_{j=1}^{M}) = \text{constant}. \tag{36}$$

The notation $\text{Cov}(\cdot)$ denotes the sample covariance matrix and $\beta_{\text{Silv.}}$ represents the KDE bandwidth parameter, computed using Silverman's Rule of Thumb [Silverman, 2018]:

$$\beta_{\text{Silv.}} = \left(\frac{4}{n_{\boldsymbol{x}}+2}\right)^{\frac{2}{n_{\boldsymbol{x}}+4}} M^{-\frac{2}{n_{\boldsymbol{x}}+4}}. \tag{37}$$

If the prediction is Gaussian from (11), then combining it with the Gaussian mixture in (35):

$$\begin{aligned} C_k\, g^{(i)}(\tilde{\boldsymbol{x}}_k) &= \int C_k\, g(\tilde{\boldsymbol{x}}_k|\boldsymbol{x}_k)\, p^{(i)}(\boldsymbol{x}_k) \mathrm{d}\boldsymbol{x}_k \\ &\approx \sum_{j=1}^{M} \frac{1}{M} \mathcal{N}(\boldsymbol{\mathcal{D}}_k^{(j)}; \hat{\boldsymbol{x}}_{k|k-1}^{(i)}, \hat{\boldsymbol{P}}_{k|k-1}^{(i)} + \boldsymbol{B}_k). \end{aligned} \tag{38}$$

Next, to maintain the requirement that each component of the GM-PHD filter remains a Gaussian after the update, the following updates them as weighted sums:

$$p^{(i)}(\boldsymbol{x}_k|\tilde{\boldsymbol{x}}_k) \approx \mathcal{N}(\boldsymbol{x}_k; \hat{\boldsymbol{x}}_{k|k}^{(i)}, \hat{\boldsymbol{P}}_{k|k}^{(i)}), \tag{39}$$

where

$$\hat{\boldsymbol{x}}_{k|k}^{(i)} = \frac{\sum_{j=1}^{M} \boldsymbol{\xi}_k^{(i,j)} \hat{\boldsymbol{\mu}}_k^{(i,j)}}{\sum_{\ell=1}^{M} \boldsymbol{\xi}_k^{(i,\ell)}} \quad \text{and} \quad \hat{\boldsymbol{P}}_{k|k}^{(i)} = \frac{\sum_{j=1}^{M} \boldsymbol{\xi}_k^{(i,j)} \hat{\boldsymbol{C}}_k^{(i,j)}}{\sum_{\ell=1}^{M} \boldsymbol{\xi}_k^{(i,\ell)}},$$

with

$$\begin{aligned} \hat{\boldsymbol{\mu}}_k^{(i,j)} &= \hat{\boldsymbol{x}}_{k|k-1}^{(i)} + \boldsymbol{K}_k^{(i,j)}(\boldsymbol{\mathcal{D}}_k^{(j)} - \hat{\boldsymbol{x}}_{k|k-1}^{(i)}), \quad \hat{\boldsymbol{C}}_k^{(i,j)} = \hat{\boldsymbol{\Sigma}}_{k|k}^{(i,j)} + (\hat{\boldsymbol{\mu}}_k^{(i,j)} - \hat{\boldsymbol{x}}_{k|k-1}^{(i)})(\hat{\boldsymbol{\mu}}_k^{(i,j)} - \hat{\boldsymbol{x}}_{k|k-1}^{(i)})^\top, \\ \hat{\boldsymbol{\Sigma}}_k^{(i,j)} &= \hat{\boldsymbol{P}}_{k|k-1}^{(i)} - \boldsymbol{K}_k^{(i,j)} \hat{\boldsymbol{P}}_{k|k-1}^{(i)}, \quad \boldsymbol{K}_k^{i,j} = \hat{\boldsymbol{P}}_{k|k-1}^{(i)} (\hat{\boldsymbol{P}}_{k|k-1}^{(i)} + \boldsymbol{B}_k)^{-1}, \quad \text{and} \\ \boldsymbol{\xi}_k^{(i,j)} &= \mathcal{N}(\boldsymbol{\mathcal{D}}_k^{(j)}; \hat{\boldsymbol{x}}_{k|k-1}^{(i)}, \hat{\boldsymbol{P}}_{k|k-1}^{(i)} + \boldsymbol{B}_k). \end{aligned}$$

Finally, in step 4 of Fig. 3, the intensity is updated by substituting (39) and (38) into (22) and (23), respectively:

$$v(\boldsymbol{x}_k|\boldsymbol{T}_k) \approx (1 - P_{D,k})v(\boldsymbol{x}_k) + \sum_{\boldsymbol{\tau}\in\boldsymbol{T}_k} \sum_{i=1}^{J_{k|k-1}} w_{k|k}^{(i)} p^{(i)}(\boldsymbol{x}_k|\tilde{\boldsymbol{x}}_k), \tag{40}$$

and,

$$w_{k|k}^{(i)} = \frac{P_{D,k} w_{k|k-1}^{(i)} \sum_{j=1}^{M} \frac{1}{M} \boldsymbol{\xi}_k^{(i,j)}}{\kappa_k(\boldsymbol{\tau}) + P_{D,k} \sum_{\ell=1}^{J_k} w_{k|k-1}^{(\ell)} \sum_{m=1}^{M} \frac{1}{M} \boldsymbol{\xi}_k^{(\ell,m)}}. \tag{41}$$

4 Numerical Experiments

In this section the proposed LS and MCMC GM-PHD filters from Section 3.4 and Section 3.5 are tested against the traditional GM-PHD filter from Vo and Ma [2006] in two examples. In the first example in Section 4.1, a mildly nonlinear system is presented, where a radar is concerned with tracking two targets that are traveling at constant velocities and cross at the exact same point in time and space. It is a mildly nonlinear system because the dynamics are linear, whereas the measurement model is nonlinear due to the radar collecting noisy and cluttered range, azimuth, and elevation measurements. While radar usually observes only one target at a time, this example is mainly included to demonstrate the generality of the proposed framework across different sensing modalities. In the second example in Section 4.2, ten debris targets in a cislunar Near Rectilinear Halo Orbit (NRHO) are being tracked by a ground-based telescope, which is pointed at apolune and provides noisy and cluttered azimuth and elevation measurements. This is a challenging example because the dynamics are strongly nonlinear and the state space is only partially observable from the measurements. Fig. 4 gives an illustration.

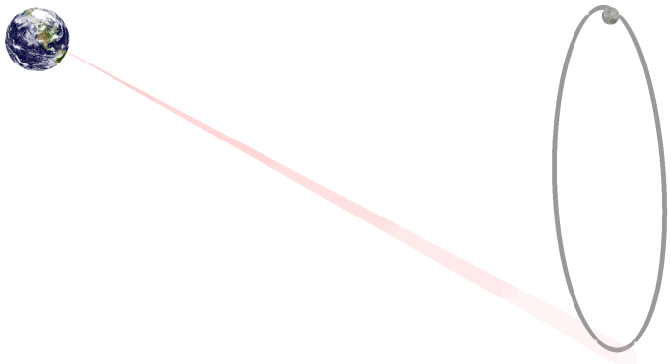

Figure 4: Illustration of the example NRHO trajectory (gray) with the telescope pointing at apolune (pink).

The nonlinear extension of the GM-PHD filter—the EK-PHD filter [Vo and Ma, 2006]—is used, but will still be referred to as the GM-PHD filter. For the LS GM-PHD filter, the MLE solution is computed using the batch LS information filter from B. Schutz [2004], which is provided in Algorithm 1 of the Appendix. It is a batch form of the Gauss-Newton algorithm and converges when the weighted root mean squared (RMS) of the measurement residuals no longer changes. The information form is preferred for systems that are over-determined where $n_{\boldsymbol{z}} > n_{\boldsymbol{x}}$ and also for systems with diffuse priors. (More details can be found in B. Schutz [2004].) As for the MCMC GM-PHD filter, this section obtains MCMC samples using HMC from Neal [2011], which is also provided in Algorithm 2 of the Appendix. HMC uses the idea of the Hamiltonian, which is separated into potential energy and kinetic energy terms. These terms are computed using the helper functions provided in Algorithms 3–6. HMC is preferred because it uses gradient information to sample from the target distribution, which reduces random walk and improves sampling efficiency. (More details can be found in Neal [2011].)

4.1 Comparison for a Mildly Nonlinear Crossing 3D Example Using Radar Measurements

4.1.1 Model Parameters

The state vector is six-dimensional:

$$\boldsymbol{x} = [\, \boldsymbol{r}_x,\, \boldsymbol{r}_y,\, \boldsymbol{r}_z,\, \boldsymbol{v}_x,\, \boldsymbol{v}_y,\, \boldsymbol{v}_z \,]^\top,$$

where $\boldsymbol{r}$ and $\boldsymbol{v}$ represent the 3-dimensional Cartesian positions and velocities relative to the origin. The motion model assumes constant velocity without process noise. The true initial states of the two targets are

$$\boldsymbol{x}_{0,1} = [\,50,\ 50,\ 50,\ 0.5,\ 0.5,\ 2\,]^\top \quad \text{and} \quad \boldsymbol{x}_{0,2} = [\,100,\ 100,\ 50,\ -0.5,\ -0.5,\ 2\,]^\top.$$

Whereas, the filters are initialized with a single low-weight component to favor births:

$$w_{0|0}^{(1)} = 1 \times 10^{-16}, \quad \hat{\boldsymbol{x}}_{0|0}^{(1)} = \mathbf{0}_{6\times 1}, \quad \text{and} \quad \hat{\boldsymbol{P}}_{0|0}^{(1)} = \boldsymbol{I}_{6\times 6},$$

where $\mathbf{0}$ represents the zero vector and $\boldsymbol{I}$ represents the identity matrix.

The measurement vector $\boldsymbol{z} = [\,\rho,\ \alpha,\ \varepsilon\,]^\top$ contains range ρ, azimuth α, and elevation ε of the observed target relative to the radar, placed at the origin. The targets remain trackable at all times. Measurements are corrupted by additive zero-mean white Gaussian noise with standard deviations of one for range and 0.5° for both azimuth and elevation. (All units are dimensionless.) Sampling occurs at a rate of $\mathrm{dt}{=}1$, starting from 0 and ending at 100. Tracklets of target detections are constructed using their respective sequences of measurements from 0–100.

Let the clutter generated state be $\boldsymbol{r}_c = [\,\boldsymbol{r}_{x,c}, \boldsymbol{r}_{y,c}, \boldsymbol{r}_{z,c}\,]^\top$, where it is Poisson distributed in the surveillance region:

$$\mathrm{S} = \{\,(\boldsymbol{r}_{x,c}, \boldsymbol{r}_{y,c}, \boldsymbol{r}_{z,c}) \mid 0 \leqslant \boldsymbol{r}_{x,c} \leqslant 200,\ 0 \leqslant \boldsymbol{r}_{y,c} \leqslant 200,\ 0 \leqslant \boldsymbol{r}_{z,c} \leqslant 400\,\},$$

with an average rate of $\lambda_C = 10$ and density $p_C = 6.25 \times 10^{-8}$. After being generated, clutter is mapped from the state space into measurements: $\boldsymbol{z}_c = h(\boldsymbol{r}_c)$. Tracklets of clutter are constructed by randomly choosing an integer between 1 and 1×10^5, and binning corresponding clutter measurements with the same integer. Although rare, this allows tracklets of clutter to still be considered and influence the outcomes of the LS and MCMC GM-PHD filters. Also for the LS and MCMC GM-PHD filters, they approximate $\kappa_k(\boldsymbol{\tau})$ using (24), which makes the assumption that shorter tracklets are more likely to be clutter:

$$\kappa_k(\boldsymbol{\tau}) = \begin{cases} 1 \times 10^8, & \text{if } |\boldsymbol{\tau}| < \left\lceil \frac{n_{\boldsymbol{x}}}{n_{\boldsymbol{z}}} \right\rceil \\ \lambda_C\, p_C\, |\boldsymbol{\tau}|^{-5n_{\boldsymbol{z}}}, & \text{otherwise} \end{cases}.$$

In the above, the ceiling ratio $\left\lceil \frac{n_{\boldsymbol{x}}}{n_{\boldsymbol{z}}} \right\rceil$ provides a rough minimum number of measurements needed to reliably estimate the target state, and tracklets shorter than this are penalized a large constant intensity 1×10^8 to discourage the filter from interpreting them as targets; otherwise, longer tracklets follow a rapidly decreasing power law, with exponent $5n_{\boldsymbol{z}}$ controlling the decay rate and multipliers $\lambda_C\, p_C$ scaling the intensity by the per-scan clutter rate and density, respectively.

The probability of detection and survival are constant such that $P_D = 0.98$ and $P_S = 0.99$, respectively. (This work does not perform measurement gating, please see Vo et al. [2015].) A Gaussian birth model is centered at the crossing point with:

$$\hat{\boldsymbol{x}}_{\gamma,k} = [\,75,\ 75,\ 150,\ 0,\ 0,\ 0\,]^\top \quad \text{and} \quad \hat{\boldsymbol{P}}_{\gamma,k} = \mathrm{diag}([\,50,\ 50,\ 50,\ 5,\ 5,\ 5\,]^2),$$

where after each prediction step, $J_{\gamma,k} = 10$ components are sampled with weights $w_{\gamma,k} = 1/100$. This model suggests that prior knowledge is given to the system that the two targets will cross. The pruning, merging, and capping parameters are 1×10^{-5}, 4, and $J_{\max} = 250$, respectively.

Both the LS and MCMC GM-PHD filters use the birth mean as their proposal mean. The MCMC GM-PHD filter uses the birth covariance to compute its HMC mass matrix $\boldsymbol{M}$. The HMC initializes with $LL{=}10$ and $\varepsilon{=}1 \times 10^{-1}$, where it collects $L{=}30$ samples and burns the first 10, so that the MCMC GM-PHD filter constructs a Gaussian mixture using $M{=}20$ samples.

4.1.2 Multi-Target Performance Metric

The Optimal Subpattern Assignment (OSPA) [Schuhmacher et al., 2008] metric evaluates tracking accuracy by measuring localization and cardinality errors between estimated states $\hat{\boldsymbol{x}}$ and ground truth $\boldsymbol{x}$. In this example, the OSPA error metric uses the Euclidean 2-norm, with parameters $p = 2$ and cutoff $c = 100$. Optimal assignments are performed using the Hungarian, *a.k.a.* Munkres, algorithm [Kuhn, 1955, Munkres, 1962]. More details on OSPA can be found in Vo and Ma [2006], Wu et al. [2023], Schuhmacher et al. [2008].

4.1.3 Results

Fig. 5 visualizes the extracted position state estimates, while Fig. 6 shows the extracted cardinality estimates. In Fig. 5(a), the red extracted state estimates fill the surveillance region in a cloud, indicating that the GM-PHD filter

struggles with the large amount of clutter and overwhelming birth model because it does not have *a priori* information about tracklets. Supporting this reasoning, Fig. 6(a) shows it failing to estimate the correct number of targets.

The LS GM-PHD filter provides estimates only at the first time step $k{=}0$, where the remainder of the extracted estimates are computed through propagation. The filter shows to favorably track the two targets in Fig. 5(b) with minimal outliers and consistent cardinality estimates in Fig. 6(b), indicating better multi-target accuracy. The MCMC GM-PHD filter fills the surveillance region with its HMC samples and also shows to favorably track the two targets in Figs. 5(c) and 6(c). Next, Fig. 7 presents the OSPA accuracy of the extracted state estimates in comparison to the truth. Corroborating the previous reasoning, both the LS and MCMC GM-PHD filters show improved accuracy over the GM-PHD filter, demonstrating that by using tracklets they both provide more informative updates that reduce the impact of clutter.

To evaluate the algorithms' relative computational costs, Fig. 8 compares their simulation wall-clock times, which is on average how long it took to run each Monte Carlo simulation. Both the LS and MCMC GM-PHD filters did not batch process separately outside of this window. Therefore their times also include the time it took them to batch process the tracklets. That said, the LS GM-PHD filter is still faster in this example than the GM-PHD filter. This can be because of a number of reasons, but mainly because 1., the LS GM-PHD filter only performs a single update, whereas the GM-PHD filter performs an update at each measurement time, and 2., LS is an efficient batch processing algorithm when given a decent proposal. Also, as expected, the MCMC GM-PHD filter takes the longest because of how inefficient the HMC algorithm is compared to LS.

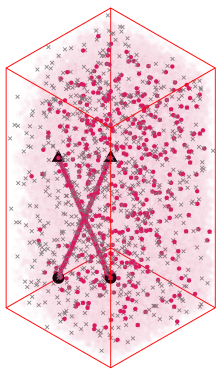

(a) GM-PHD

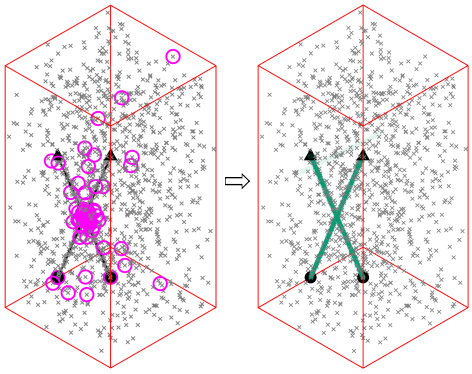

(b) LS batch solutions (left), LS GM-PHD (right)

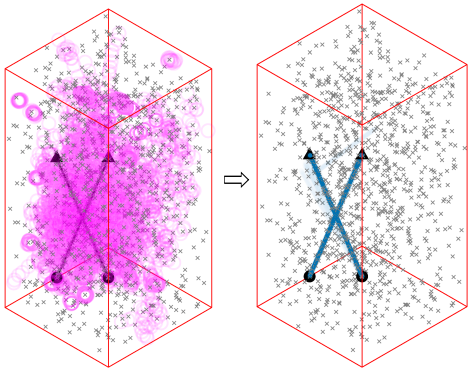

(c) MCMC batch solutions (left), MCMC GM-PHD (right)

Figure 5: These figures show the three-dimensional true trajectories of the two targets (black), the batch solution positions (fuchsia circles), and the extracted position estimates of the compared filters (red, green, and blue dots). These are the results of a single chosen Monte Carlo simulation. The transparent dots represent the extracted position estimates from the remaining Monte Carlo simulations. Measurements consist of target detections and clutter (gray crosses), with clutter modeled as a Poisson process uniformly distributed over the surveillance region (red box).

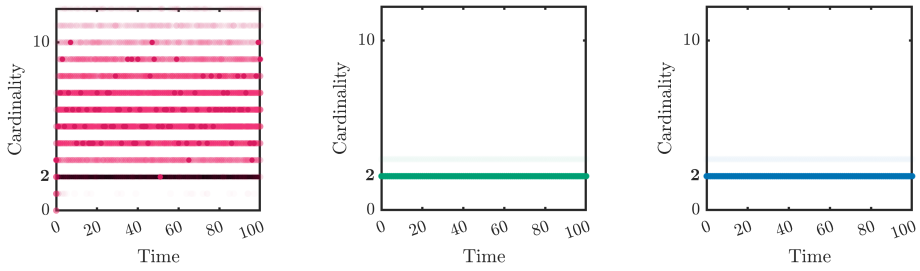

(a) GM-PHD (b) LS GM-PHD (c) MCMC GM-PHD

Figure 6: These figures show the true target cardinality (black) and the extracted cardinality estimates of the compared filters over time (red, green, and blue dots). These are the results of 250 Monte Carlo simulations.

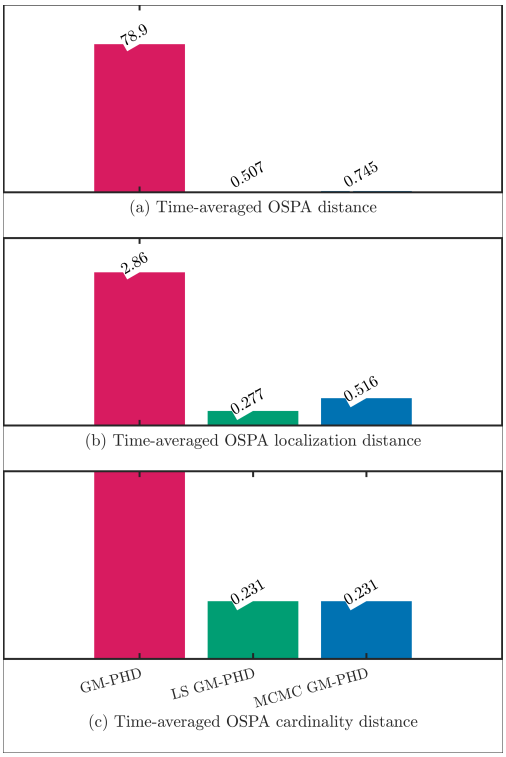

Figure 7: This figure shows the multi-target accuracy (OSPA) of each filter averaged over time. Results are further averaged over 250 Monte Carlo simulations.

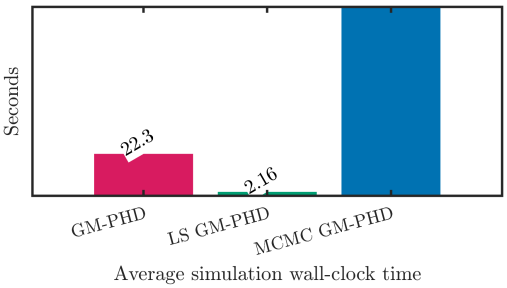

Figure 8: This figure shows the simulation wall-clock times of each filter. Results are averaged over 250 Monte Carlo simulations. Using MATLAB with an Intel Core i7 9700K CPU at a base speed of 3.00 GHz and with 16 GB of RAM.

4.2 Comparison for a Strongly Nonlinear Cislunar Debris Tracking Example Using Angles-Only Measurements

4.2.1 Model Parameters

The dynamics are modeled using the Circular Restricted Three Body Problem (CR3BP) for the Earth-Moon system:

$$\dot{\boldsymbol{r}}(1)=\boldsymbol{v}(1), \quad \dot{\boldsymbol{r}}(2)=\boldsymbol{v}(2), \quad \dot{\boldsymbol{r}}(3)=\boldsymbol{v}(3),$$

$$\dot{\boldsymbol{v}}(1)=\boldsymbol{r}(1)+2\boldsymbol{v}(2)-\frac{(1-\mu)(\boldsymbol{r}(1)+\mu)}{r_{\oplus}^3}-\frac{\mu(\boldsymbol{r}(1)-1+\mu)}{r_{\leftmoon}^3}, \quad \dot{\boldsymbol{v}}(2)=\boldsymbol{r}(2)-2\boldsymbol{v}(1)-\frac{(1-\mu)\boldsymbol{r}(2)}{r_{\oplus}^3}-\frac{\mu\boldsymbol{r}(2)}{r_{\leftmoon}^3}, \quad \text{and}$$

$$\dot{\boldsymbol{v}}(3)=-\frac{(1-\mu)\boldsymbol{r}(3)}{r_{\oplus}^3}-\frac{\mu\boldsymbol{r}(3)}{r_{\leftmoon}^3},$$

where $\boldsymbol{r}$ and $\boldsymbol{v}$ represent the scaled Cartesian positions and velocities of the target with respect to the barycenter origin. The parameter μ is the scaled Moon geocentric gravitational constant, and $r_{\oplus}$ and $r_{\leftmoon}$ are the distances of the target with respect to the Earth and Moon in the barycenter reference frame:

$$\mu = \frac{\mu_{\leftmoon}}{\mu_{\oplus}+\mu_{\leftmoon}}, \quad r_{\oplus} = \sqrt{(\boldsymbol{r}(1)+\mu)^2 + \boldsymbol{r}(2)^2 + \boldsymbol{r}(3)^2}, \quad \text{and}$$
$$r_{\leftmoon} = \sqrt{(\boldsymbol{r}(1)-1+\mu)^2 + \boldsymbol{r}(2)^2 + \boldsymbol{r}(3)^2}.$$

In this example, $\mu_{\oplus} = G \cdot m_{\oplus}$ and $\mu_{\leftmoon} = G \cdot m_{\leftmoon}$. The gravitational constant is $G = 6.6743 \times 10^{-11}\ \mathrm{m^3\,s^{-2}\,kg^{-1}}$, the mass of the Earth is $m_{\oplus} = 5.972 \times 10^{24}$ kg, and the mass of the Moon is $m_{\leftmoon} = 7.342 \times 10^{22}$ kg. The units for distance and time are normalized by length units $\mathrm{LU} = 384\,400 \times 10^3$ m and time units $\mathrm{TU} = \sqrt{\mathrm{LU}^3/\left(\mu_{\oplus}+\mu_{\leftmoon}\right)}$ s. The system dynamic equations are numerically integrated with an embedded Runge-Kutta 8(7) method [Dormand and Prince, 1980]. Before the simulation begins, the following state $\boldsymbol{x}_0$ is propagated forward by 95% of its orbital period:

$$\boldsymbol{x}_0 = [\,1.0110350588,\ 0,\ -0.1731500000,\ 0,\ -0.0780141199,\ 0\,]^{\top},$$

which has an orbital period of $\mathrm{T} = 1.3632096570$. Then, the ten targets are Gaussian distributed on top of the resulting propagated state, with covariance:

$$\boldsymbol{P}_0 = \mathrm{diag}([\,6\times10^{-4},\ 6\times10^{-4},\ 6\times10^{-4},\ 1\times10^{-6},\ 1\times10^{-6},\ 1\times10^{-6}\,]^2).$$

The telescope itself is located at the Earth-Moon barycenter and pointed in the direction of $\boldsymbol{x}_0(1{:}3)$. It has an exposure window that lasts $10\mathrm{h}$, which starts at the beginning of each orbital period for four periods. During this window, measurements are recorded at a rate of $\mathrm{dt}{=}1\mathrm{h}$. The measurement vector $\boldsymbol{z} = [\,\alpha,\ \varepsilon\,]^{\top}$ contains azimuth α and elevation ε of the observed target relative to the barycenter origin. Measurements of actual targets are collected whenever a target crosses the telescope's field of view $\mathrm{fov}{=}0.5^{\circ}$. The measurements are corrupted by additive zero-mean white Gaussian noise with 1σ azimuth and elevation uncertainties of 16.1 arc-seconds for both. (Measurement biases and time delay due to light travel are not considered.) For each exposure window, tracklets of target detections are constructed using their respective sequences of measurements.

Let the clutter be denoted $\boldsymbol{z}_c = [\,\alpha_c,\ \varepsilon_c\,]^{\top}$, where it is Poisson distributed in the surveillance region:

$$\mathrm{S}{=}\left\{ (\alpha_c,\ \varepsilon_c) \,\middle|\, -\frac{\mathrm{fov}}{2}{\leqslant}\alpha_c{\leqslant}+\frac{\mathrm{fov}}{2},\ -\frac{\mathrm{fov}}{2}{\leqslant}\varepsilon_c{\leqslant}+\frac{\mathrm{fov}}{2} \right\}$$

with an average rate of $\lambda_C{=}1$ and uniform density $p_C{=}1.313 \times 10^4$. Tracklets of clutter are constructed by randomly choosing an integer between 1 and 1×10^5, and binning corresponding clutter measurements with the same integer. Although rare, this allows tracklets of clutter to still be considered and influence the outcomes of the LS and MCMC GM-PHD filters. Also for the LS and MCMC GM-PHD filters, the clutter intensity function $\kappa_k(\boldsymbol{\tau})$ is constructed the same as the previous example.

The probability of detection is $P_D = 0.9$ and the probability of survival is $P_S = 0.99$. A Gaussian birth model is centered at apolune:

$$\hat{\boldsymbol{x}}_{\gamma,k} = [\,\boldsymbol{x}_0(1),\ \boldsymbol{x}_0(2),\ \boldsymbol{x}_0(3),\ 0,\ 0,\ 0\,]^{\top} \quad \text{and} \quad \hat{\boldsymbol{P}}_{\gamma,k} = \boldsymbol{P}_0,$$

where after each prediction step, $J_{\gamma,k} = 10$ components are sampled with weights $w_{\gamma,k} = 1/10$. This model suggests that prior knowledge is given to the system that the two targets will appear in the telescope's pointed direction. The pruning, merging, and capping parameters are 1×10^{-8}, 3, and $J_{\max} = 100$, respectively. The filters are initialized with a single low-weight component to favor births:

$$w_{0|0}^{(1)} = 1 \times 10^{-16}, \quad \hat{\boldsymbol{x}}_{0|0}^{(1)} = \hat{\boldsymbol{x}}_{\gamma,k}, \quad \text{and} \quad \hat{\boldsymbol{P}}_{0|0}^{(1)} = \hat{\boldsymbol{P}}_{\gamma,k}.$$

Both the LS and MCMC GM-PHD filters use the birth mean as their proposal mean. The MCMC GM-PHD filter uses the birth covariance to compute its HMC mass matrix $\boldsymbol{M}$. The HMC initializes with $LL{=}20$ and $\varepsilon{=}1 \times 10^{-3}$, where it collects $L{=}30$ samples and burns the first 10, so that the MCMC GM-PHD filter constructs a Gaussian mixture using $M{=}20$ samples. In this example, the OSPA error metric uses the Euclidean 2-norm, with parameters $p = 2$ and cutoff $c = 10,000\text{km}$.

4.2.2 Results

Fig. 9 visualizes the extracted position state estimates, while Fig. 10 shows the extracted cardinality estimates. In Fig. 9(a), the red extracted state estimates occur towards the end of the target trajectories and span the unobservable range and range rate directions. This indicates that the GM-PHD filter struggles to update using individual measurements. Supporting this reasoning, Fig. 6(a) shows it failing to underestimate the correct number of targets.

The LS GM-PHD filter provides estimates at the first time step of each exposure window, where the remainder of the extracted estimates are computed through propagation and evaluation of whether the propagated estimates are within the telescope's field of view. (This is post-processing that an operator might perform.) The filter shows to favorably track the ten targets for their full trajectories in Fig. 5(b), but struggles to estimate in the unobservable range and range rate directions. This is likely because the LS batch solution, which is a single mean with covariance, is insufficient in capturing the non-Gaussianities of the measurements. The MCMC GM-PHD filter, on the other hand, does a good job at collecting samples in the range and range rate directions in Figs. 5(c). Then, by approximating the measurement distribution as a Gaussian mixture, the MCMC GM-PHD filter is able to better capture the non-Gaussianities, and therefore resulting in more accurate estimates.

Next, Fig. 11 presents the OSPA accuracy of the extracted state estimates in comparison to the truth. Corroborating the previous reasoning, both the LS and MCMC GM-PHD filters show improved accuracy over the GM-PHD filter, demonstrating that they both provide more informative updates that reduce the impact of clutter. Then, to evaluate the algorithms' relative computational costs, Fig. 12 compares their simulation wall-clock times, which is on average how long it took to run each Monte Carlo simulation. Although, both the LS and MCMC GM-PHD filters did not batch process separately outside of this window, the LS GM-PHD filter is still faster in this example than the GM-PHD filter. However, as expected, the MCMC GM-PHD filter takes the longest because of how inefficient the HMC algorithm is compared to LS. Overall, the results show that, while the MCMC GM-PHD filter is slower, it obtains better multi-target accuracy than both the GM-PHD and LS GM-PHD filters for more complex systems.

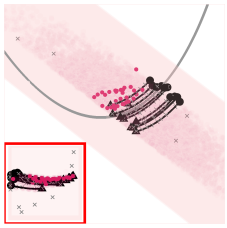

(a) GM-PHD

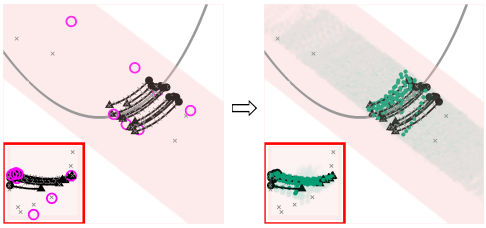

(b) LS batch solutions (left), LS GM-PHD (right)

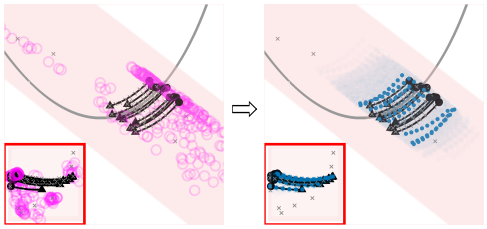

(c) MCMC batch solutions (left), MCMC GM-PHD (right)

Figure 9: These figures show the three-dimensional true trajectories of the ten targets (black), the batch solution positions (fuchsia circles), and the extracted position estimates of the compared filters (red, green, and blue dots). These are the results of a single chosen Monte Carlo simulation from the third orbit pass. The transparent dots represent the extracted position estimates from the remaining Monte Carlo simulations. Measurements consist of target detections and clutter (gray crosses), with clutter modeled as a Poisson process uniformly distributed over the surveillance region (red square).

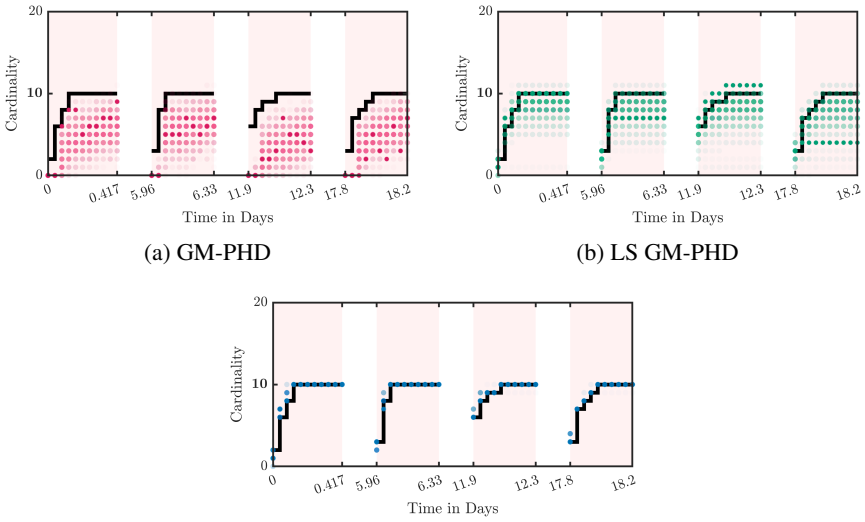

(a) GM-PHD (b) LS GM-PHD

(c) MCMC GM-PHD

Figure 10: These figures show the true target cardinality (black) and the extracted cardinality estimates of the compared filters over time (red, green, and blue dots). The pink regions represent the periodic 10h exposure windows during which targets pass through the telescope's field of view. These are the results of 250 Monte Carlo simulations encompassing all four orbit passes.

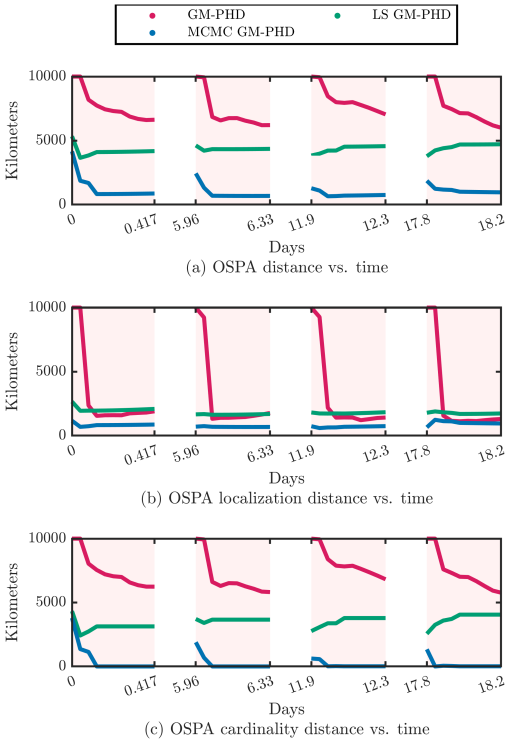

(a) OSPA distance vs. time

(b) OSPA localization distance vs. time

(c) OSPA cardinality distance vs. time

Figure 11: This figure shows the multi-target accuracy (OSPA) of each filter over time. The pink regions represent the periodic 10h exposure windows during which targets pass through the telescope's field of view. Results are averaged over 250 Monte Carlo simulations.

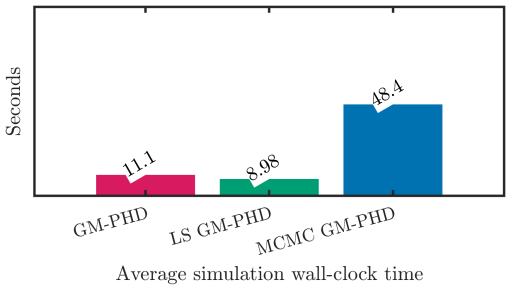

Average simulation wall-clock time

Figure 12: This figure shows the simulation wall-clock times of each filter. Results are averaged over 250 Monte Carlo simulations. Using MATLAB with an Intel Core i7 9700K CPU at a base speed of 3.00 GHz and with 16 GB of RAM.

5 Conclusion

This article presents a Random Finite Set (RFS) framework for batch processing tracklets in the Gaussian Mixture Probability Hypothesis Density (GM-PHD) filter. Unlike the traditional GM-PHD filter, which updates recursively with individual sensor measurements, the proposed approach updates using tracklets, which reduces the impact of clutter and improves multi-target filtering (MTF) performance. To achieve this, the proposed approach updates the GM-PHD filter's posterior intensity function by pre-processing tracklets into a batch solution of the state space, where the batch solution is then treated as a noisy measurement of the multi-target state.

To apply this approach to practical examples, we use two different methods for batch processing. Least Squares (LS) is used to batch process tracklets into a mean and covariance for mildly nonlinear and nearly Gaussian-shaped systems, whereas Markov Chain Monte Carlo (MCMC) with Kernel Density Estimation (KDE) is used to batch process tracklets into Gaussian mixtures for more strongly nonlinear systems, resulting in the LS GM-PHD filter and the MCMC GM-PHD filter, respectively. While less efficient than LS, the MCMC GM-PHD filter better captures non-Gaussian measurement uncertainties and recovers missing state information.

The proposed LS and MCMC GM-PHD filters are tested against the traditonal GM-PHD filter in a crossing 3D example using radar measurements and in a cislunar debris tracking example using angles-only measurements. While there are some differences in performance, the overall results show that both the LS and MCMC GM-PHD filters improve MTF accuracy, demonstrating that they provide more informative updates and reduce the impact of clutter, compared to the traditional GM-PHD filter.

The differences in performance between the LS and MCMC GM-PHD filters are primarily from how each method represents uncertainty. The LS approach linearizes the measurement model and assumes nearly Gaussian-shaped probability distributions, which is sufficient when the system dynamics and measurement models are only mildly nonlinear and locally observable, like in the radar tracking example. But for more complex systems, like the cislunar debris tracking example, the probabilities become more non-Gaussian in shape and LS can no longer represent this complexity with a single mean and covariance. The MCMC with KDE approach, on the other hand, is able to directly sample from the true likelihood and preserve the full non-Gaussian structure of the uncertainty, but at the expense of being less computationally efficient. Therefore, the LS GM-PHD filter is preferred for low-nonlinearity applications, whereas the MCMC GM-PHD filter is more suitable when accuracy under strong nonlinearity outweighs computational efficiency.

To improve the computational speed of the MCMC GM-PHD filter, future directions should consider more efficient MCMC sampling algorithms instead of Hamiltonian Monte Carlo (HMC). Additionally, since the LS and MCMC GM-PHD filters use tracklets rather than individual measurements, the clutter intensity becomes a function of the tracklets. Therefore, future directions should also consider developing accurate and tractable approximations of this clutter intensity.

Appendix. Algorithms

Algorithm 1: Batch Least Squares Information Filter.

Given: $\boldsymbol{x}_k^{\text{Prop.}}$ (proposal mean), $\boldsymbol{\tau}_k{=}\{\boldsymbol{z}_\ell\}_{\ell\in\boldsymbol{\mathcal{I}}_{\boldsymbol{\tau}_k}}$ (tracklet), $\boldsymbol{R}$ (meas. covariance), ε (threshold).

Initialize: $\hat{\boldsymbol{x}}_k{=}\boldsymbol{x}_k^{\text{Prop.}}$, $\delta\bar{\boldsymbol{x}}_k{=}\boldsymbol{0}$, $\text{rms}_{\text{prev.}}{=}0$, $\text{rms}{=}\varepsilon{+}1$.

Repeat until $\text{abs}(\text{rms}-\text{rms}_{\text{prev.}})\leqslant\varepsilon$:
  $\bar{\boldsymbol{x}}_\ell{\leftarrow}\hat{\boldsymbol{x}}_k$, $\boldsymbol{\Lambda}_k{\leftarrow}\boldsymbol{0}$, $\boldsymbol{N}_k{\leftarrow}\boldsymbol{0}$, $\boldsymbol{F}_{\ell|k}{\leftarrow}\mathbb{I}_{n_{\boldsymbol{x}}\times n_{\boldsymbol{x}}}$, $\text{rms}_{\text{prev.}}\leftarrow\text{rms}$, $\nu\leftarrow 0$
  For each ℓ in $\boldsymbol{\mathcal{I}}_{\boldsymbol{\tau}_k}$:
    $\boldsymbol{F}_{\ell|\ell}{\leftarrow}\frac{\partial f(\boldsymbol{x})}{\partial\boldsymbol{x}}\big|_{\boldsymbol{x}=\bar{\boldsymbol{x}}_\ell}$, $\boldsymbol{F}_{\ell|k}{\leftarrow}\boldsymbol{F}_{\ell|\ell}\boldsymbol{F}_{\ell|k}$, $\bar{\boldsymbol{x}}_\ell{\leftarrow}f(\bar{\boldsymbol{x}}_\ell)$
    $\hat{\boldsymbol{z}}_\ell\leftarrow h(\bar{\boldsymbol{x}}_\ell)$, $\boldsymbol{H}_\ell\leftarrow\frac{\partial h(\boldsymbol{x})}{\partial\boldsymbol{x}}\big|_{\boldsymbol{x}=\bar{\boldsymbol{x}}_\ell}$
    $\boldsymbol{\Lambda}_k\leftarrow\boldsymbol{\Lambda}_k+\left(\boldsymbol{F}_{\ell|k}\right)^\top(\boldsymbol{H}_\ell)^\top(\boldsymbol{R})^{-1}\boldsymbol{H}_\ell\boldsymbol{F}_{\ell|k}$
    $\boldsymbol{N}_k\leftarrow\boldsymbol{N}_k+\left(\boldsymbol{F}_{\ell|k}\right)^\top(\boldsymbol{H}_\ell)^\top(\boldsymbol{R})^{-1}(\boldsymbol{z}_\ell-\hat{\boldsymbol{z}}_\ell)$
    $\nu\leftarrow\nu+(\boldsymbol{z}_\ell-\hat{\boldsymbol{z}}_\ell)^\top(\boldsymbol{R})^{-1}(\boldsymbol{z}_\ell-\hat{\boldsymbol{z}}_\ell)$
  $\delta\hat{\boldsymbol{x}}_k\leftarrow(\boldsymbol{\Lambda}_k)^{-1}\boldsymbol{N}_k$
  $\hat{\boldsymbol{x}}_k\leftarrow\hat{\boldsymbol{x}}_k+\delta\hat{\boldsymbol{x}}_k$, $\delta\bar{\boldsymbol{x}}_k\leftarrow\delta\bar{\boldsymbol{x}}_k-\delta\hat{\boldsymbol{x}}_k$
  $\text{rms}\leftarrow(\nu/|\boldsymbol{\mathcal{I}}_{\boldsymbol{\tau}_k}|)^{1/2}$

Output: $\hat{\boldsymbol{x}}_k$ (estimated mean), $(\boldsymbol{\Lambda}_k)^{-1}$ (estimated covariance).

Algorithm 2: Batch Hamiltonian Monte Carlo.

Given: $\boldsymbol{x}_k^{\text{Prop.}}$ (proposal mean), $\boldsymbol{P}_k^{\text{Prop.}}$ (proposal covariance), $\boldsymbol{\tau}_k{=}\{\boldsymbol{z}_\ell\}_{\ell\in\boldsymbol{\mathcal{I}}_{\boldsymbol{\tau}_k}}$ (tracklet), $\boldsymbol{R}$ (meas. covariance), L (number of samples), LL (leapfrog steps), ε (HMC step size).

Initialize: $q{=}\boldsymbol{x}_k^{\text{Prop.}}$, $\boldsymbol{M}{=}(\boldsymbol{P}_k^{\text{Prop.}})^{-1}$, accept = 0, $\tilde{\boldsymbol{x}}_k{=}\varnothing$.

Repeat until accept $=L$:
  $q^*\leftarrow q$, $p^*\sim\mathcal{N}(\boldsymbol{0},\boldsymbol{M})$, $p\leftarrow p^*$
  $p^*\leftarrow p^*-\varepsilon\nabla U(q^*,\boldsymbol{\tau}_k,\boldsymbol{R})/2$
  Iterate LL times:
    $q^*\leftarrow q^*+\varepsilon\nabla K(p^*,\boldsymbol{M})$
    If not last iteration, Then:
      $p^*\leftarrow p^*-\varepsilon\nabla U(q^*,\boldsymbol{\tau}_k,\boldsymbol{R})$
  $p^*\leftarrow p^*-\varepsilon\nabla U(q^*,\boldsymbol{\tau}_k,\boldsymbol{R})/2$
  $p^*\leftarrow -p^*$
  If rand $\leqslant\min\big(1,\exp(U(q,\boldsymbol{\tau}_k,\boldsymbol{R})-U(q^*,\boldsymbol{\tau}_k,\boldsymbol{R})+K(p,\boldsymbol{M})-K(p^*,\boldsymbol{M}))\big)$,
  Then:
    $q{\leftarrow}q^*$, $\varepsilon{\leftarrow}\varepsilon{*}1.2$, $\tilde{\boldsymbol{x}}_k{\leftarrow}\tilde{\boldsymbol{x}}_k{\cup}q$, accept$+{=}1$
  Else:
    $\varepsilon\leftarrow\varepsilon/1.2$

Output: $\tilde{\boldsymbol{x}}_k$ (MCMC samples).

Algorithm 3: HMC Helper Function, $U(\cdot)$.

Given: q (position), $\boldsymbol{\tau}_k{=}\{\boldsymbol{z}_\ell\}_{\ell\in\boldsymbol{\mathcal{I}}_{\boldsymbol{\tau}_k}}$ (tracklet), $\boldsymbol{R}$ (meas. covariance).

Initialize: $\nu\leftarrow 0$.

For each ℓ in $\boldsymbol{\mathcal{I}}_{\boldsymbol{\tau}_k}$:
  $q\leftarrow f(q)$, $\hat{\boldsymbol{z}}_\ell\leftarrow h(q)$, $\boldsymbol{H}_\ell\leftarrow\frac{\partial h(\boldsymbol{x})}{\partial\boldsymbol{x}}\big|_{\boldsymbol{x}=q}$
  $\nu\leftarrow\nu+(\boldsymbol{z}_\ell-\hat{\boldsymbol{z}}_\ell)^\top(\boldsymbol{R})^{-1}(\boldsymbol{z}_\ell-\hat{\boldsymbol{z}}_\ell)$

Output: $U{=}\nu{+}|\boldsymbol{\mathcal{I}}_{\boldsymbol{\tau}_k}|\big[\log\left((2\pi)^{n_{\boldsymbol{z}}/2}\det((\boldsymbol{R})^{1/2})\right)\big]$ (potential energy).

Algorithm 4: HMC Helper Function, $\nabla U(\cdot)$.

Given: q (position), $\boldsymbol{\tau}_k{=}\{\boldsymbol{z}_\ell\}_{\ell\in\boldsymbol{\mathcal{I}}_{\boldsymbol{\tau}_k}}$ (tracklet), $\boldsymbol{R}$ (meas. covariance).

Initialize: $\boldsymbol{N}_k{\leftarrow}\boldsymbol{0}$, $\boldsymbol{F}_{\ell|k}{\leftarrow}\mathbb{I}_{n_{\boldsymbol{x}}\times n_{\boldsymbol{x}}}$.

For each ℓ in $\boldsymbol{\mathcal{I}}_{\boldsymbol{\tau}_k}$:
  $\boldsymbol{F}_{\ell|\ell}\leftarrow\frac{\partial f(\boldsymbol{x})}{\partial\boldsymbol{x}}\big|_{\boldsymbol{x}=q}$, $\boldsymbol{F}_{\ell|k}\leftarrow\boldsymbol{F}_{\ell|\ell}\boldsymbol{F}_{\ell|k}$, $q\leftarrow f(q)$
  $\hat{\boldsymbol{z}}_\ell\leftarrow h(q)$, $\boldsymbol{H}_\ell\leftarrow\frac{\partial h(\boldsymbol{x})}{\partial\boldsymbol{x}}\big|_{\boldsymbol{x}=q}$
  $\boldsymbol{N}_k\leftarrow\boldsymbol{N}_k+\left(\boldsymbol{F}_{\ell|k}\right)^\top(\boldsymbol{H}_\ell)^\top(\boldsymbol{R})^{-1}(\boldsymbol{z}_\ell-\hat{\boldsymbol{z}}_\ell)$

Output: $\nabla U=-\boldsymbol{N}_k$ (gradient of the potential energy).

Algorithm 5: HMC Helper Function, $K(\cdot)$.

Given: p (momentum), $\boldsymbol{M}$ (mass covariance).

Output: $K=-\log\left(\mathcal{N}(p;\boldsymbol{0},\boldsymbol{M})\right)$ (kinetic energy).

Algorithm 6: HMC Helper Function, $\nabla K(\cdot)$.

Given: p (momentum), $\boldsymbol{M}$ (mass covariance).

Output: $\nabla K=(\boldsymbol{M})^{-1}p$ (gradient of the kinetic energy).

Acknowledgments

This material is based on research sponsored by the Air Force Office of Scientific Research (AFOSR) under agreement number FA9550-23-1-0646, *Create the Future Independent Research Effort (CFIRE)*.

References

Neal A Carlson. Federated filter for multiplatform track fusion. In *Signal and Data Processing of Small Targets*, volume 3809, pages 320–331. SPIE, 1999. doi:10.1117/12.364031.

Oliver E Drummond. Track fusion with feedback. In *Signal and Data Processing of Small Targets*, volume 2759, pages 342–360. SPIE, 1996. doi:10.1117/12.241196.

Oliver E Drummond. Track and tracklet fusion filtering. In *Signal and Data Processing of Small Targets*, volume 4728, pages 176–195. SPIE, 2002. doi:10.1117/12.478532.

Oliver E Drummond and David Dana-Bashian. Comparison of tracklet filter methods for non-maneuvering targets. In *Signal and Data Processing of Small Targets*, volume 5913, pages 455–467. SPIE, 2005. doi:10.1117/12.624911.

HS Satz and TH Kerr. Comparison of batch and Kalman filtering for radar tracking. In *Proceedings of 10th Annual AIAA/BMDO Conference*, 2001. URL `https://apps.dtic.mil/sti/html/tr/ADP011192/`.

Dalton Durant, Andrey A Popov, and Renato Zanetti. MCMC EnGMF for sparse data orbit determination. In *2023 AAS/AIAA Astrodynamics Specialist Conference*, pages 23–356, 2023.

Dalton Durant, Andrey A Popov, and Renato Zanetti. Processing angles-only tracklets for cislunar multi-target tracking. In *2024 AAS/AIAA Astrodynamics Specialist Conference*, pages 24–339, 2024.

B-N Vo and W-K Ma. The Gaussian mixture probability hypothesis density filter. *IEEE Transactions on Signal Processing*, 54(11):4091–4104, 2006. doi:10.1109/TSP.2006.881190.

Yong Qin, Hong Ma, Jinfeng Chen, and Li Cheng. Gaussian mixture probability hypothesis density filter for multipath multitarget tracking in over-the-horizon radar. *EURASIP Journal on Advances in Signal Processing*, 2015:1–18, 2015. doi:10.1186/s13634-015-0294-y.

Martin Tobias and Aaron D Lanterman. Probability hypothesis density-based multitarget tracking with bistatic range and doppler observations. *IEE Proceedings-Radar, Sonar and Navigation*, 152(3):195–205, 2005. URL `https://digital-library.theiet.org/doi/abs/10.1049/ip-rsn%3A20045031`.

Volker Eiselein, Daniel Arp, Michael Pätzold, and Thomas Sikora. Real-time multi-human tracking using a probability hypothesis density filter and multiple detectors. In *2012 IEEE 9th International Conference on Advanced Video and Signal-Based Surveillance*, pages 325–330. IEEE, 2012. doi:10.1109/AVSS.2012.59.

Nam Trung Pham, Weimin Huang, and SH Ong. Probability hypothesis density approach for multi-camera multi-object tracking. In *Computer Vision–ACCV 2007: 8th Asian Conference on Computer Vision, Tokyo, Japan, November 18-22, 2007, Proceedings, Part I 8*, pages 875–884. Springer, 2007. doi:10.1007/978-3-540-76386-4_83.

Christian Lundquist, Lars Hammarstrand, and Fredrik Gustafsson. Road intensity based mapping using radar measurements with a probability hypothesis density filter. *IEEE Transactions on Signal Processing*, 59(4):1397–1408, 2010. doi:10.1109/TSP.2010.2103065.

Keith YK Leung, Felipe Inostroza, and Martin Adams. Relating random vector and random finite set estimation in navigation, mapping, and tracking. *IEEE Transactions on Signal Processing*, 65(17):4609–4623, 2017. doi:10.1109/TSP.2017.2701330.

Dalton Durant, Uwe D Hanebeck, and Renato Zanetti. Good things come to those who weight! Improving Gaussian mixture weights for cislunar debris tracking. In *35th AAS/AIAA Space Flight Mechanics Meeting*, pages 25–309, 2025.

Kyle J DeMars and James S McCabe. Tracking of the LANDSAT 2 rocket body primary breakup. In *25th AAS/AIAA Space Flight Mechanics Meeting*, pages 15–420, 2015.

Brandon A Jones, Daniel S Bryant, Ba-Tuong Vo, and Ba-Ngu Vo. Challenges of multi-target tracking for space situational awareness. In *2015 18th International Conference on Information Fusion (Fusion)*, pages 1278–1285. IEEE, 2015. URL `https://ieeexplore.ieee.org/abstract/document/7266704`.

Giovanni Lavezzi. *Image processing of multiclass satellite tracklets for initial orbit determination based on optical telescopes*. PhD thesis, Master's thesis, Politecnico di Milano, 2018. URL `https://www.politesi.polimi.it/handle/10589/139506?mode=simple`.

Ronald PS Mahler. Multitarget Bayes filtering via first-order multitarget moments. *IEEE Transactions on Aerospace and Electronic systems*, 39(4):1152–1178, 2003. doi:10.1109/TAES.2003.1261119.

Rudolph Emil Kalman. A new approach to linear filtering and prediction problems. *Journal of Basic Engineering*, 82 (1):35–45, 1960. ISSN 0021-9223. doi:10.1115/1.3662552.

B. Tapley B. Schutz, G. Born. *Statistical Orbit Determination*. Elsevier Academic Press, 2004. ISBN 9780080541730.

Nicholas Metropolis, Arianna W Rosenbluth, Marshall N Rosenbluth, Augusta H Teller, and Edward Teller. Equation of state calculations by fast computing machines. *The Journal of Chemical Physics*, 21(6):1087–1092, 1953. ISSN 0021-9606. doi:10.1063/1.1699114.

W Keith Hastings. Monte Carlo sampling methods using Markov chains and their applications. *Biometrika*, 57(1): 97–109, 04 1970. ISSN 0006-3444. doi:10.1093/biomet/57.1.97.

Radford M Neal. MCMC using Hamiltonian dynamics. In Steve Brooks, Andrew Gelman, Galin Jones, and Xiao-Li Meng, editors, *Handbook of Markov Chain Monte Carlo*, pages 113–162. CRC Press, 2011. doi:10.1201/b10905.

Bernard W Silverman. *Density Estimation for Statistics and Data Analysis*. Routledge, 2018. doi:10.1201/9781315140919.

Ba-Ngu Vo, Mahendra Mallick, Yaakov Bar-Shalom, Stefano Coraluppi, Richard Osborne, Ronald Mahler, and Ba-tuong Vo. Multitarget tracking. *Wiley Encyclopedia of Electrical and Electronics Engineering*, 2015. URL `https://ba-ngu.vo-au.com/vo/VMBCOMV_MTT_WEEE15.pdf`.

Dominic Schuhmacher, Ba-Tuong Vo, and Ba-Ngu Vo. A consistent metric for performance evaluation of multi-object filters. *IEEE Transactions on Signal Processing*, 56(8):3447–3457, 2008. doi:10.1109/TSP.2008.920469.

Harold W Kuhn. The Hungarian method for the assignment problem. *Naval Research Logistics Quarterly*, 2(1-2): 83–97, 1955. doi:10.1002/nav.3800020109.

James Munkres. Algorithms for the assignment and transportation problems. *Society for Industrial and Applied Mathematics*, 15:196–210, 1962. doi:10.1137/0105003.

Weihua Wu, Hemin Sun, Mao Zheng, and Weiping Huang. *Target Tracking with Random Finite Sets*. Springer, 2023. doi:10.1007/978-981-19-9815-7.

John R Dormand and Peter J Prince. A family of embedded Runge-Kutta formulae. *Journal of Computational and Applied Mathematics*, 6(1):19–26, 1980. doi:10.1016/0771-050X(80)90013-3.